The Australian Summertime Cool Change. Part II: Mesoscale Aspects

J. R. GARRATT AND W. L. PHYSICK

CSIRO Division of Atmospheric Research, Melbourne

R. K. SMITH

Geophysical Fluid Dynamics Laboratory, Monash University, Melbourne

A. J. TROUP[1]

(Manuscript received 29 December 1983, in final form 6 August 1984)

ABSTRACT

Observations of four cold-frontal systems traversing the coastal region of southeast Australia in late spring and early summer are described in terms of processes occurring on the mesoscale. A conceptual model is presented which summarizes the main results of the data analysis. Features found in common with other studies of cold fronts include:

(i) the multiple-line nature of the frontal transition zone (FTZ);
(ii) concentration of cyclonic relative vorticity at a height $z \approx 1$ to 1.5 km in the rear of the FTZ; and
(iii) the existence of a prefrontal jet at $z \approx 1.5$ km, northerly in our case, southerly in the Northern Hemisphere.

The change lines within the FTZ (and at the leading edge if there is no sea breeze) are most probably convective instability lines whose alignment and movement depend on the large-scale, cloud-layer winds. The lines are evident as mesoscale cloud bands from satellite imagery and as rainbands from radar. At least one of these develops into a vigorous squall line whose cold outflow produces a pressure jump, and related wind-shift line. Movement of the pressure-jump line depends both on the gravity-current nature of the cold outflow and the environmental wind field. The squall line and pressure-jump line are associated with mesoscale high and low pressure features to which the boundary-layer wind field responds.

The structure of the FTZ up to $z = 2$ km appears to be dominated by the presence of the squall line, with upwards motion ahead and downwards behind. On a horizontal scale of 100 km, cyclonic vorticity reaches twice the Coriolis parameter f in the vicinity of the squall line. Frontogenesis occurs largely within the FTZ with horizontal convergence and deformation processes being of comparable importance.

The prefrontal jet is broadly in thermal wind balance with the horizontal temperature gradient which is, itself, determined by the fact that prefrontal air closest to the FTZ originates farther to the north and is therefore hotter than prefrontal air more distant from the zone.

1. Introduction

Early mesoanalyses of severe storms recognized the importance of "disturbances with linear dimensions of 10–100 miles" (Fujita, 1955), which more or less defined "mesoscale" from the observational viewpoint. Some years later Orlanski (1975) defined mesoscale to cover horizontal wavelengths of 2–2000 km, with subdivisions of meso-α (200–2000 km), meso-β (20–200 km) and meso-γ (2–20 km). The meso-β range then corresponds with Fujita's earlier identified scale, although Fujita (1981) has recently proposed a modified scheme and defined mesoscale for the range 4–400 km. More recently, with the work of Emanuel (1979; 1982) for example, "mesoscale" has been given dynamical as well as observational significance, particularly as it applies to prefrontal squall lines. The study of frontal mesoscale processes described in the present paper is confined more or less to the meso-β scale. Orlanski (1975) gave examples of meso-β phenomena which included the nocturnal low-level jet, squall lines and cloud clusters, all of which are relevant to the present study.

The significance of the meso-β scale to the dynamics of cold fronts and squall lines is readily apparent from past studies. Early observational work showed a dynamically active region of width ~100 km associated with the prefrontal squall line (Newton 1950), with individual large cumulonimbus (Cb) and Cb-lines having related surface mesopressure features of horizontal dimension ~10–100 km (e.g., Fujita, 1963). More recently, Hoxit *et al.* (1976) have discussed the presence of meso-β scale vertical circula-

[1] We dedicate this paper to the memory of Sandy Troup, whose contribution to the Cold Fronts Research Programme was considerable. His recent untimely death is a loss to the Programme and to his many colleagues in Meteorology.

tions in the vicinity of large Cb and squall lines, while Fritsch and Chappell (1980) gave an example of observed convectively driven pressure systems of scale ~100 km (their Fig. 1). In studies of extratropical cyclones and cold fronts, significant meso-β and meso-γ scale structures have been revealed, including the prefrontal low level jet (Browning and Pardoe, 1973) and rainbands embedded in the frontal region (James and Browning, 1979; Hobbs *et al.*, 1980).

The Northern Hemisphere studies carry several obvious implications for summertime frontal systems in southeast Australia. Firstly, the moist warm flow associated with the prefrontal low-level jet in the Northern Hemisphere would be replaced by a hot, dry flow with possible effects on the intensity of "line convection" (Browning and Harrold, 1970; Hobbs *et al.*, 1980) and on reduced rainfall arising from that convection. Second, frictional convergence ahead of the surface cold front would be affected by the presence of the coastline, more so at these latitudes (35–40°S) than for the United Kingdom for example (50–55°N) because of the deeper and more frequently occurring convective boundary layer over land.

Frontal studies in Australia have been confined mostly to summertime "cool changes" in southeastern Australia (Berson *et al.*, 1957, 1959; Berson, 1958; Clarke, 1961) and are the subject of a recent review by Ryan (1982). These disturbances, manifest as one or more surface discontinuities, were related to the passage of cold fronts, sea-breeze fronts and pressure-jump lines associated with gravity waves traveling on an elevated inversion. The influence of strong daytime heating over the land on the diurnal variation of speed of movement and of times of arrival of the leading discontinuity was clearly demonstrated. Of particular relevance to the present study was the identification of a transition zone between warm and cold air, with relatively strong surface convergence and shear (Berson *et al.*, 1957).

The aims of the Cold Fronts Research Programme are described by Smith *et al.* (1982), the main emphasis being concerned with the meso-α (called here subsynoptic) and meso-β (mesoscale) processes. Specifically we seek to extend both our knowledge of Australian frontal systems, and of frontal systems in general, by comparison with known features of Northern Hemisphere systems. We will be particularly concerned with the surface and lower tropospheric nature of the transition zone, and of the origin, lifetime and evolutionary characteristics of mesoscale systems existing within it.

The plan of the paper is as follows: In Section 2 we describe briefly the mesonetwork and data base used in the study, Section 3 describes the physical features of the frontal transition zone and Section 4 examines the structure of the kinematic fields, including the rate of frontogenesis. In Section 5 the low-level wind field is described, and features of the squall line and associated cold outflow are discussed in Section 6. Finally, a conceptual mesoscale model of the FTZ is presented in Section 7.

2. Cold Fronts Research Programme—field phases

The Experiment comprized two Phases held during the period mid-November to mid-December (late spring/early summer) in 1980 and 1981. In all, seven observing periods (called Events), each of duration 16–30 h, were associated with frontal-like systems bringing significant changes in some or all of wind speed and direction, temperature, humidity and pressure at the surface and in the lowest few kilometers of the troposphere (see Wilson and Stern, 1985). The study is confined to four of these frontal systems (mainly Events 2, 3 and 4 of Phase 2, with some reference made to Event 1 of Phase 1) for which sufficiently comprehensive data for detailed analysis were available. These events show many common features including the presence of a squall line and rainbands embedded in a fairly well-defined transition zone between hot, dry northerly winds and cool southwesterly winds. This type of frontal system probably constitutes the most common found during early summer, and represents a significant forecasting problem in southeast Australia.

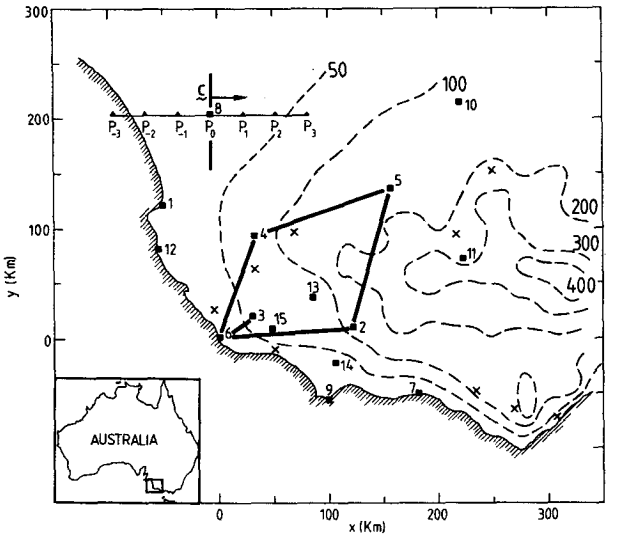

FIG. 1. Mesonetwork showing main (numbers 1 to 15) and subsidiary (crosses) stations. Dashed lines are topographic contours in meters. North-south heavy line through station 8 represents the "change line" traveling from west to east at speed c. Time series of pressure observations used in the pressure-field analysis are extrapolated forwards and backwards in time at 30 min intervals; the equivalent positions in space at station 8 are shown as closed triangles for $c = 16.7$ m s^{-1}. Thus p_0 represents the pressure at $t = t_0$ (map time), p_1 is observation at $t_0 - 30$ min, p_2 at $t_0 - 60$ min, p_3 at $t_0 - 90$ min, p_{-1} at $t_0 + 30$, p_{-2} at $t_0 + 60$ min, p_{-3} at $t_0 + 90$ min where the spacing $\Delta x = c\Delta t$ and $\Delta t = 30$ min. Heavy outline defines the 5-station array.

The main network of 15 stations (Phase 2) was confined to an area of approximately 300 km square, with the central station at Mount Gambier airport (designated Station 3) located at 37°44.7'S, 140°46.5'E. The location of these stations, together with subsidiary stations used in isochronology analysis, are shown in Fig. 1. Additional stations and raingages were utilized in the study outside of the area shown, particularly in the Melbourne region. The heavy outline shows the 5 balloon-ascent stations used in the wind and wind-derivative analyses. Details of observations made at each station are given in Table 1.

Surface data (u and v are wind components; T is temperature; q is specific humidity and p is pressure) were available for analysis at 3 min or 30 min intervals throughout each designated frontal event, with pressures compensated for their known long-term diurnal variation. In contrast, upper air wind data from the 3 pibal stations were made at 30–60 min intervals, mostly to 1.5–2.5 km, and wind and temperature data from the two upper-air stations were available for the most part at 2 hour intervals throughout each event.

Radar (10 cm) PPI data in the form of 16 mm film were available from Mount Gambier, with a range of approximately 200 km. These were analyzed each 15–30 min when available (not during the 1 hour or so of any upper-air flight), and supplemented by the Melbourne radar to provide continuity right through the region between Mount Gambier and Melbourne. Visual and infrared cloud pictures were available at 3 hourly intervals from the Japanese geostationary meteorological satellite (GMS).

The research F27 aircraft flew one or two 4-hour sorties over both sea and land during most events, giving selected horizontal and vertical profiles of wind and thermodynamic variables.

Data analysis procedures and some details on the mesoscale pressure field analysis are described in the Appendix.

Times are usually given in Greenwich Mean Time (GMT); local times (daylight saving) are 10½ and 11 hours ahead of GMT in South Australia and Victoria, respectively.

3. Frontal transition zone—physical features

a. Isochronology

Examination of surface observations, with appropriate correlation in space of significant discontinuities, usually reveals several "change lines" in the prefrontal region (i.e., ahead of the surface cold front), which delineate the transition zone between hot northerlies and cool southwesterlies. This frontal transition zone (FTZ) can be interpreted more or less as the prefrontal trough ahead of the surface cold front, a term in common use among practicing meteorologists in Australia. The change lines themselves are identified by significant surface pressure changes, wind shifts and/or temperature falls in such a way that the isochrones of these changes behave

TABLE 1. Details of stations and observations. Type of observation:

p_3	Digital pressure observations each 3-min
p_{30}	Daily barograph reduced to observations each 30-min
V	Anemograph observations of wind speed and direction at 2 m or 10 m height—digitized to 5 or 10 min values
T	Thermohygrograph observations reduced to observations each 30-min
R	PPI radar observations
W	Pibal observations.
U	Upper-air observations
A	Base for aircraft observations.

	Observations							
Station	p_3	p_{30}	V	T	W	U	R	A
1 Kingston	p_3		V					
2 Branxholme	p_3		V	T	W			
3 Mount Gambier	p_3		V	T		U	R	A
4 Struan	p_3		V	T	W			
5 Horsham	p_3		V	T		U		
6 Pelican Point	p_3		V	T	W			
7 Warrnambool		p_{30}						
8 Keith		p_{30}		T				
9 Cape Nelson		p_{30}	V					
10 Birchip		p_{30}	V	T				
11 Ararat		p_{30}		T				
12 Robe				T				
13 Casterton			V	T				
14 Heywood				T				
15 Rennick				T				

consistently. Directions and speeds of movement of these "lines" can then be estimated across the mesonetwork, and often through to the Melbourne region. They are designated throughout the paper as D_1, D_2, $\cdots$, D_f, D_f being the final change line of a frontal system conventionally analyzed as the surface cold front.

1) CHANGE LINES OVER THE LAND

The prefrontal stream of warm northerly air was disturbed by an *initial change line* (D_1) identified by a leveling or rising of the pressure which had been previously falling, and an associated backing of the wind; for a sea breeze, the backing is large, accompanied by a significant temperature fall near the coast. The nature of this leading line depends strongly on the time of day, and hence on the likely presence of sea breezes. If no sea breeze is present, the line will probably correspond with a small pressure jump and wind shift, both coincident with the passage of the leading edge of a middle-level cloud band (a weak convective instability line). The onset of cold, steady southwesterly winds some hours later occurs with passage of the *final or trailing change line* (D_f) often identified additionally by a steady pressure rise behind the line. In the seven events observed, D_f could be so identified in the majority of cases; in the remainder, the final change was gradual. The region between the initial and final lines constitutes the FTZ, in which a sequence of intermediate change lines (D_2, D_3, $\cdots$), mostly associated with pressure jumps generated by one or more squall lines[2], are revealed.

The multiple-line nature of the frontal transition zone was revealed initially by Berson *et al.* (1957, 1959) and we shall frequently revert to their terminology, particularly in relation to the transition zone. Our observations reveal that in the Mount Gambier region this may be several hundred kilometers in width, and oriented between northwest–southeast and north–south. In six out of the seven events analyzed, the initial change line arrived at the coast at Station 6 between 1730 and 0400 GMT (i.e., between 0400 and 1430 local time), confirming the diurnal influence on the movement of frontal systems found by Berson *et al.*

Over land the speed of movement of the *initial line* was ~ 12 m s^{-1} if associated with a convective instability line and ~ 5 m s^{-1} if a sea breeze; the *final line* generally moved at a speed of ~ 10–15 m s^{-1}. Intermediate lines, particularly the main pressure jump, tended to move through the transition zone at speeds ~ 15–25 m s^{-1}. As we shall see, the majority of the change lines were often related to the presence of squall lines, and consequently to the associated meso pressure features at the surface.

Change lines identified at the surface were always accompanied by cooling and wind changes aloft, often to 1–3 km in height. For intermediate lines cooling was solely associated with evaporation of rain into unsaturated air, while strong backing of the wind was associated with passage of the main pressure-jump line. In most cases, rain or virga was associated with lines enabling the relation between surface isochrones of wind and temperature changes and radar echoes to be examined.

Figures 2a and 2b give an example of the coincidence of surface isochrones with radar echoes and

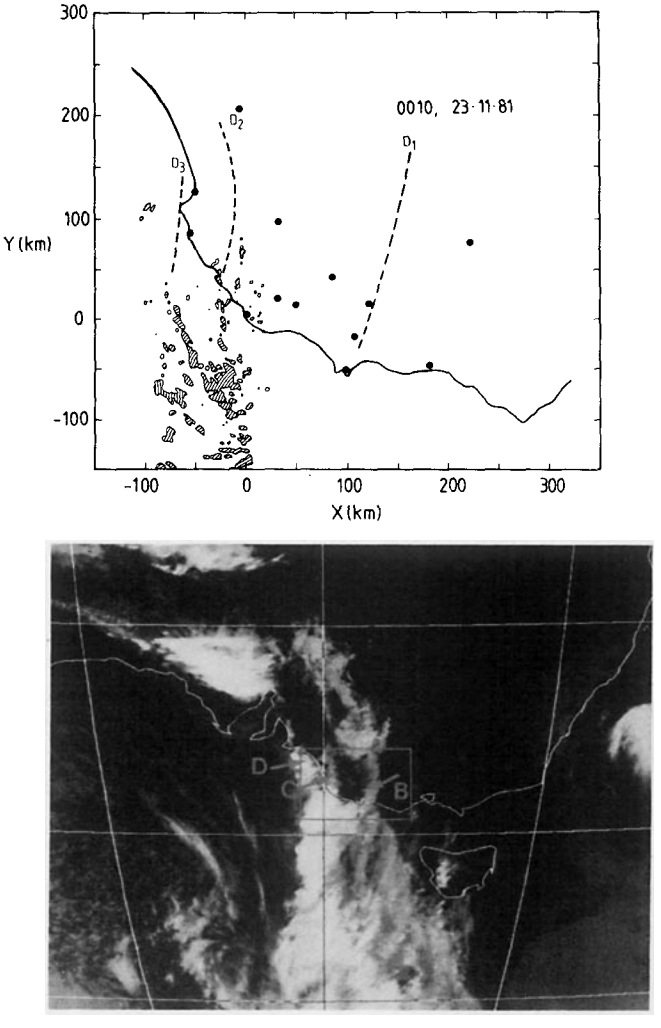

FIG. 2. (a) Surface isochrones of change lines (extrapolation over the sea based on pressure-field analysis) and radar echoes; (b) GMS infrared cloud distribution illustrating relation between surface lines and radar/cloud bands for Event 2 at 0000 GMT 23 November 1981. See text for the five cloud bands, A–E.

[2] Squall line refers to a line of Cb, and heavy precipitation forming along the downdraft "squall front"—see Houze (1977) and Zipser (1977). It is an example of an intense convective instability line.

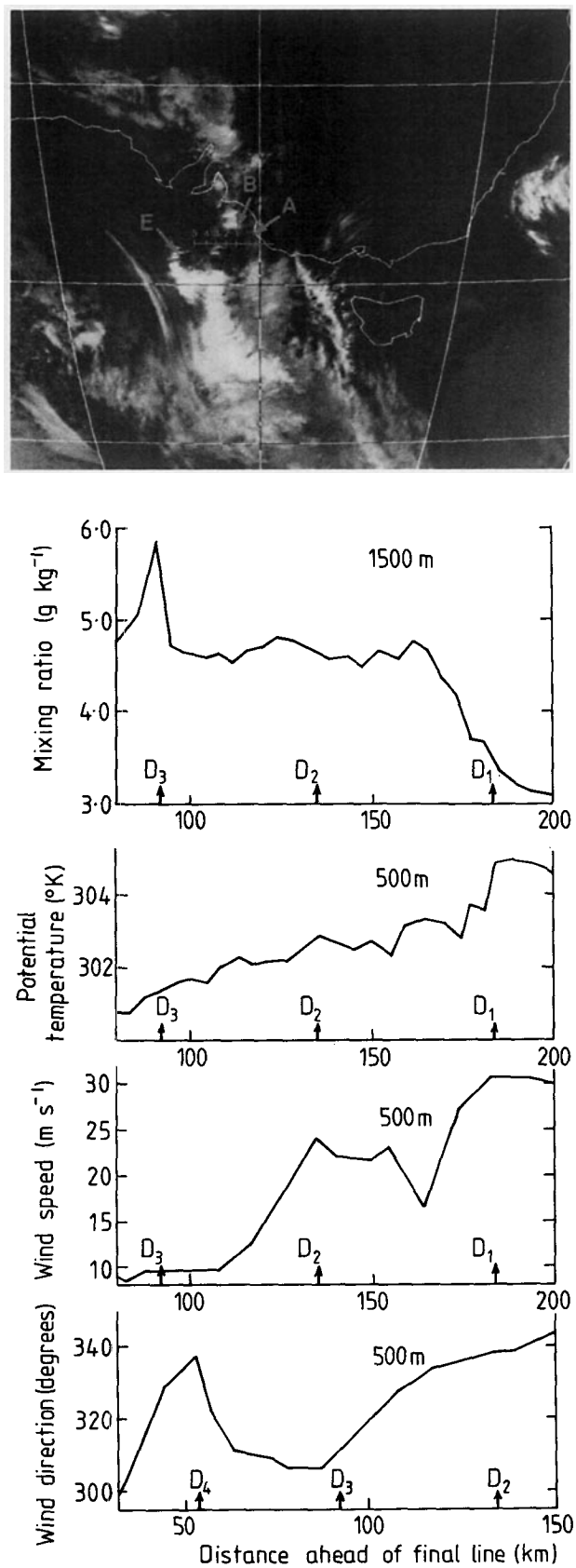

band structure in the GMS cloud distribution. Lines D_1 and D_2 correspond with the rear edges of cloud bands *B* and *C*, with line D_3 associated with cloud band *D*. At this time no obvious organization in the radar echoes associated with cloud bands *C* and *D* was evident. The most northwesterly echoes in Fig. 2a evolved into an echo band associated with cloud band *D* and a further line D_4. By 0200 GMT three fairly distinct radar echo bands had formed and by 0400 GMT these had combined to give one major band corresponding to the pressure-jump line D_4; see evolution in Fig. 7. During this time, however, extensive cirrus cover prevented any identification of middle-level bands from GMS imagery.

2) Change lines over the sea

The relationship between radar echo bands, cloud bands and surface change lines observed over land (e.g., Fig. 2) suggests that where such bands occur earlier over the sea, analogous discontinuities might be found over the land. This is confirmed by aircraft observations out to several hundred kilometers from the coast, though the specific discontinuity is not always in the same form as observed subsequently over land; see Section 7 and the discussion on coastal influence.

A good example is shown in Figs. 3a,b which precedes the situation in Fig. 2 by about 6 h, and shows the existence of lines D_1 to D_4 and several corresponding cloud bands. Line D_4, identified by significant backing of the wind, ultimately develops into a major squall line over land. Cloud bands *A* and *E* dissipated in the 6 h period following the situation in Fig. 3.

b. Convective instability lines and rainbands

Mesoscale cloud bands correspond mostly with active organized convection and occur sometimes as substructure in a synoptic-scale band constituting the prefrontal region (e.g., see Figs. 2 and 3). Where the convection is sufficiently intense with cumulonimbi present, they can be interpreted as squall lines. In practice these coincide with rainbands identified from PPI radar scans and with low-level change lines constituting the FTZ. The convective lines may be more or less continuous over several hundreds of kilometers, though not always visible as such from satellite or radar. Where gaps occur, surface observations confirmed the presence of a line of nonprecipitating Cu convection.

FIG. 3. (a) GMS cloud distribution for Event 2 at 1800 GMT 22 November 1981 showing the aircraft flight path and positions of the five change lines. (b) Corresponding horizontal variations of properties through the FTZ over the ocean, between the first and the final line at flight levels of 500 and 1500 m.

The existence of these convective lines is probably related to the presence of strong vertical shear and may be a type of inertial (symmetric) instability of the stably-stratified, but conditionally unstable, shear flow to two-dimensional mesoscale perturbations (e.g., Emanuel, 1979, 1982, and the reviews by Lilly, 1979, and Houze and Hobbs, 1982). Symmetric baroclinic instability has been proposed also as a possible explanation for frontal rainbands (Bennetts and Hoskins, 1979). Our particular interest lies in the factors determining the orientation of the lines (particularly the main squall lines), their speed of movement and, at the mesoscale, their influence on the structure of the FTZ.

The relationship of severe storms and squall lines to vertical wind shear has received considerable attention in the literature; the problem of shear and squall-line alignment less so (see Emanuel, 1982, p. 1092; Lilly, 1979, pp. 131, 156). According to these authors, squall lines tend to be aligned parallel to the low-level shear, but our observations indicate only a weak correlation of alignment with the shear between near-surface and 2 km. However, the observed squall lines in this study are mostly associated with cold fronts and aligned approximately parallel to, and ahead of, the surface cold front. The alignment of the latter, and hence that of the associated squall lines, is strongly related to the cloud-layer shear [between 2 (±1) km and 6.5 (±1.5) km]. In this case we find the shear vector is, on average, normal to the line. Figure 4 shows the wind vectors and the squall-line position for each of the major events under study. These results reflect to a great extent those of Elliott and Hovind (1964) who studied convective rainbands in extra-tropical storms crossing California. In contrast the prefrontal squall line case discussed by Held (1977) in South Africa showed that the cloud-layer shear (2 to 8 km) lay parallel to the squall line.

The FTZ may be comprised of *one to three* convective lines, and considerable evolution or decay of these in terms of squall-line development, particularly as revealed from radar PPI, occurs in the area. Most of the thunderstorm activity is confined to within 150 km either side of the coastline (e.g., as illustrated in Fig. 7). The speed V_s of the squall lines varies considerably, typical values being 5–20 m s^{-1}, similar to values for the Northern Hemisphere (Boucher and Wexler 1961). Our observations indicate that this speed is determined by the mean-wind vector, say $\bar{\mathbf{V}}$, for the layer approximately between 2 and 7 km, and the squall-line alignment. The individual storm cells are steered to a large extent by $\bar{\mathbf{V}}$, at an angle ϵ to the squall-line, whence we expect $V_s \approx |\bar{\mathbf{V}}| \sin\epsilon$. The relation is shown in Fig. 5 where V_s, ϵ have been estimated from radar echo-band movement and $\bar{\mathbf{V}}$ from upper winds.

Precipitation occurrence and amounts for each rainband and squall line were typically <5 mm in total, and occurrence and duration of precipitation at any one location corresponded generally with the passage of the radar-echo band. The lack of substantial rainfall amounts at the surface is presumably related to the prefrontal influx of dry continental air at low levels, leading to evaporation of rain and hence the cold outflows observed in the lowest few km (see Section 6).

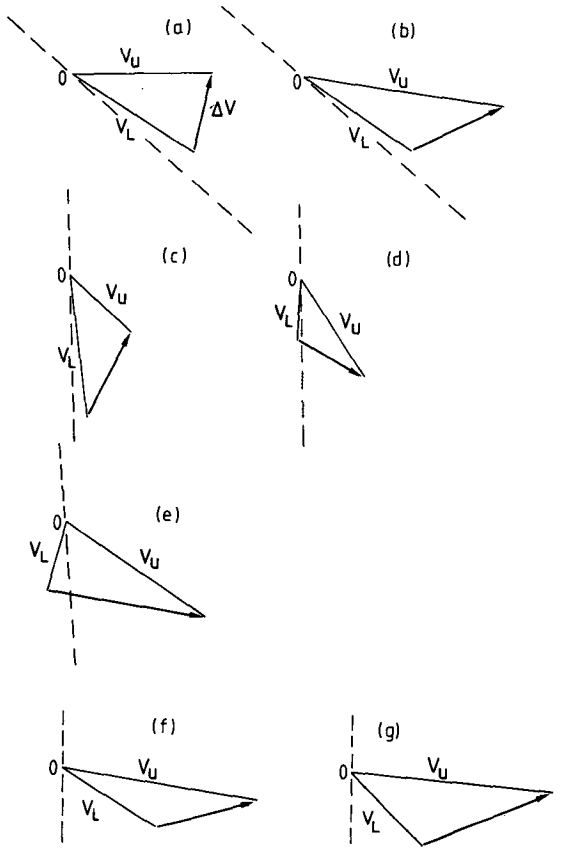

FIG. 4. Relationship between the cloud-layer shear vector (ΔV) and squall-line alignment, the latter being represented by the dashed line in each case. Winds are constructed from the origin at 0, with the low-level wind $\mathbf{V}_L$ referred to z = 2.1–2.3 km and upper level-wind $\mathbf{V}_U$ to z = 6.2–7.3 km (exact value of z is chosen for convenience only). Examples (a) Event 1 at 1440 GMT (Station 3); (b) Event 1 at 1835 GMT (3); (c) Event 2 at 1835 GMT (3); (d) Event 2 at 2235 GMT (5); (e) Event 3 at 0635 GMT (3); (f) Event 4 at 0435 GMT (3); (g) Event 4 at 0435 GMT (5).

c. *Mesoscale pressure field*

Observations in the United States emphasize the remarkable association between squall lines and strong mesoscale pressure disturbances near the surface (e.g., Fujita, 1955; Hoxit *et al.*, 1976). Figure 6 shows for Event 2 the time sequence of surface pressure at six stations in the network during passage of the FTZ, within which a major squall line evolved. Positions of surface change lines are shown, together with

significant pressure features (mesohighs H1, H2, · · · and mesolows L1, L2, · · ·). United States studies suggest that the mesohigh is related to the squall-line outflow. The pressure jump is then associated with the passage of the leading edge of this outflow which is identified with the "gust front" (e.g., Fujita 1963). In an isolated system, the downwind mesolow, usually 50–100 km distant from the main mesohigh, is related hydrostatically to subsidence warming in the upper troposphere induced by a vertical meso-circulation normal to the squall line (Hoxit *et al.*, 1976; Fritsch and Chappell, 1980). As an example of these mesoscale features we show two pressure fields separated by 2 hours with radar echoes superimposed (Fig. 7). Note that the main meso-pressure features are typically 50 to 100 km in size which is the transverse scale of the squall line itself. Furthermore, the sharp changes in pressure evident in station time traces shown in Fig. 6, and generally corresponding to change lines (e.g., as in Fig. 2), are smoothed out in the space fields due to the data sampling procedure (see Appendix).

In the example shown, rainbands at 0200 GMT have become organized in the coastal region (compare with the echoes at 0000 GMT approximately shown in Fig. 2) and have an associated weak mesohigh H1. By 0400 GMT the region is dominated by the main squall line, with associated "bubble mesohigh" H2, downwind mesolow L2 and possible "wake low" L3 (see Koch and McCarthy, 1982). These features are particularly evident on the station 6 time trace in Fig. 6.

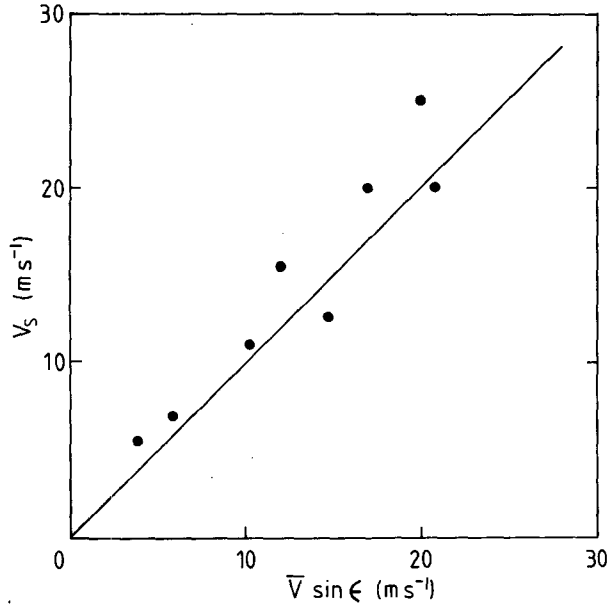

FIG. 5. Relationship between V_s, the squall-line/rainband speed as determined from radar echo-band movement, and the observed cloud-layer winds given by $\overline{V}$ sin ϵ.

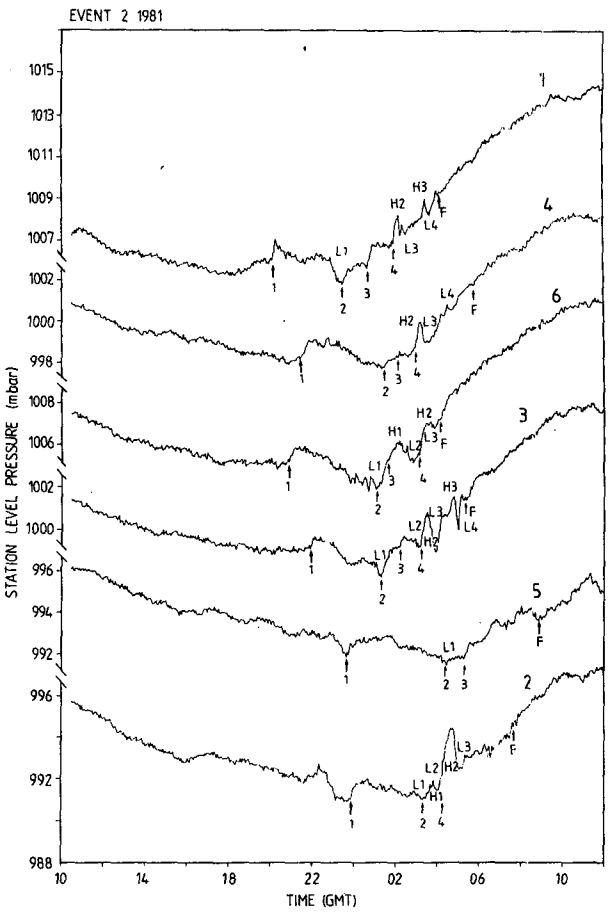

FIG. 6. Time series of surface pressure for six stations (1 to 6) during passage of frontal system (Event 2) on 22–23 November 1981. Symbols 1 . . . F show time of passage of change lines; mesohighs and mesolows are represented by H1, H2 . . . and L1, L2. . . .

The distribution of mesopressure features across the network, on the above and other occasions, is reminiscent of the large meso-β features shown in Fig. 1a of Hoxit *et al.* (1976), Fig. 1 of Fritsch and Chappell (1980), both associated with squall lines, and of the small meso-β features described by Koch and McCarthy (1982) in relation to mesoconvective systems along the Oklahoma dryline.

d. Thermal stability and baroclinity

Observations of thermal structure suggest:

(i) an FTZ characterized by a mixed layer 1–3 km deep, with considerable variation in its depth across the zone;

(ii) at night time, a shallow stably-stratified pre-frontal boundary layer (<0.5 km deep) and associated nocturnal jet at 250–500 m; and

(iii) a shallow convective post-frontal mixed layer (0.5–1 km deep).

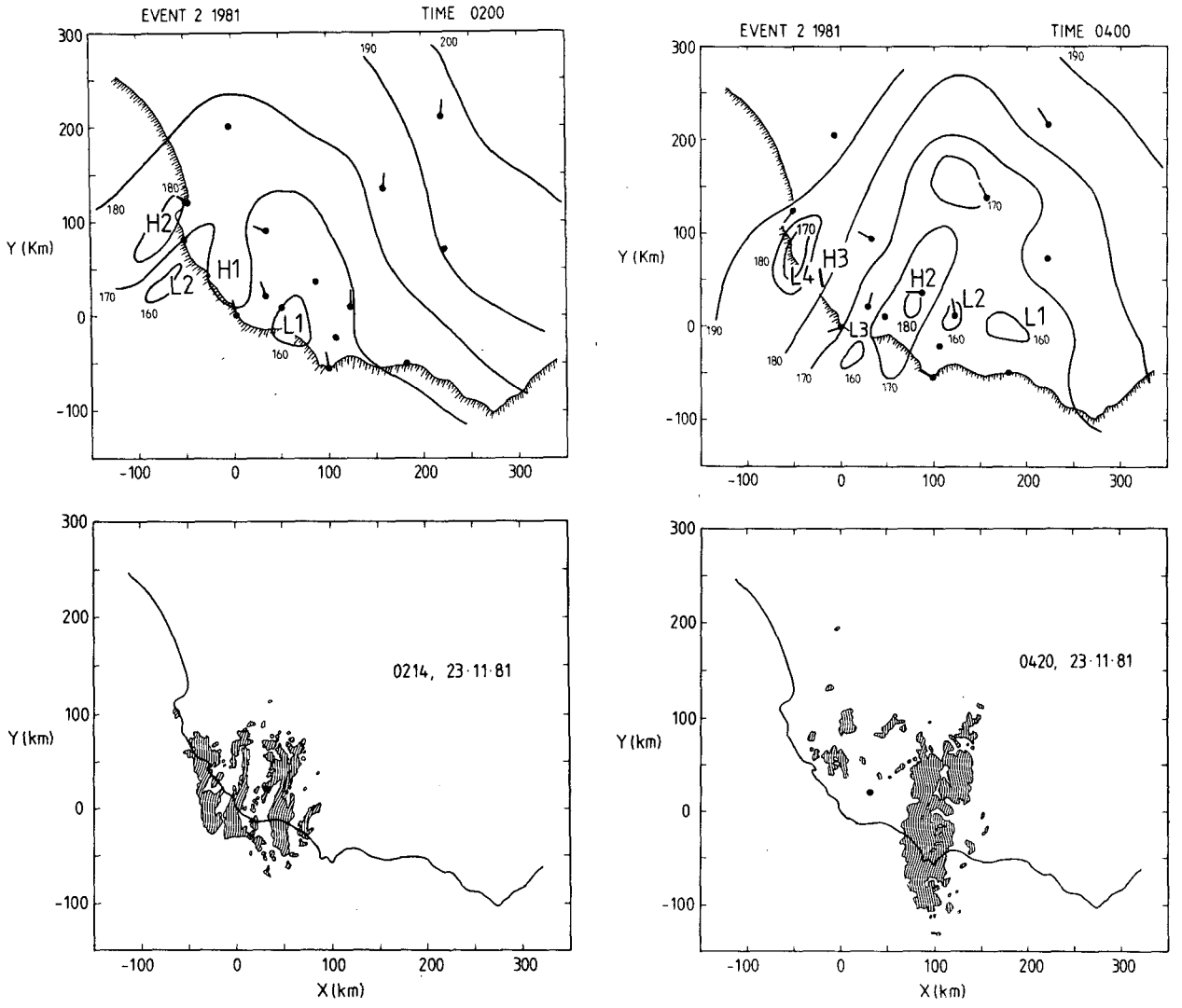

FIG. 7. Mesopressure fields for frontal system Event 2 on 23 November 1981 at 0200 GMT and 0400 GMT with pressures shown in tenths of a millibar above 990 mb. Direction of surface winds is shown at several stations and beneath the pressure fields the main radar echoes are presented.

All of these features are consistent with the time of arrival of the initial line at Station 6 between 0730 and 1430 local time for the four events analysed.

At heights up to at least 1 km, the horizontal temperature gradient[3] is positive within, and concentrated to the rear of, the FTZ as evidenced in the two examples shown in Fig. 8. Here the field in Fig. 8a corresponds to the pressure field given in Fig. 7b, while Fig. 8b illustrates the case of a strong cold outflow from a squall line. In the latter event the leading line at this time, D_3 represents pressure jumps associated with two outflows—one due to the squall line in the coastal region and the other to storms to the north that have dissipated and therefore are not visible on radar.

Ahead of the FTZ, though not shown in the Fig. 8, there is a region of negative temperature gradient (up to height ~ 1 km); i.e., temperature decreasing away from the FTZ towards the east. This has implications for the low-level wind field (see Section 5).

4. Kinematic fields

a. Vorticity and vertical motion fields

Time-height cross sections of the vertical component of relative vorticity $\zeta(z, t)$ and vertical velocity $w(z, t)$ in the lowest two kilometers are shown in Figs. 9 and 10, respectively, for Events 2, 3 and 4.

[3] $\partial T/\partial x'$ is defined relative to rectangular axes x', y' where the positive x' axis is normal to the front and pointing towards the warm air; see legend of Fig. 12.

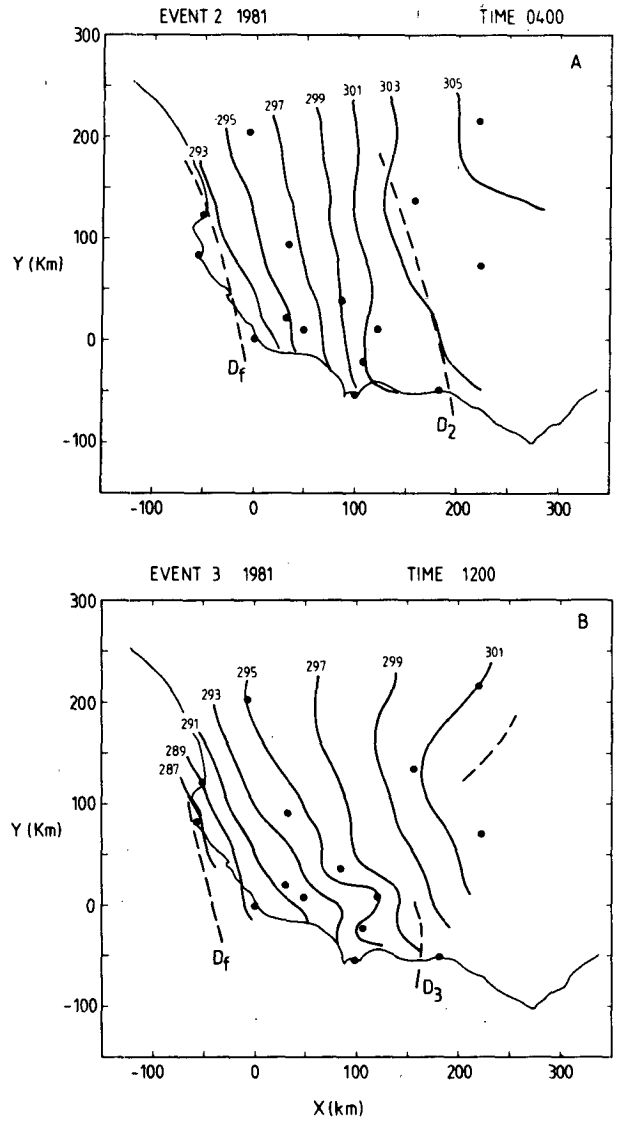

FIG. 8. Surface isentropes during passage of the FTZ: (a) 0400 GMT 23 November 1981 and (b) 1200 GMT 27 November 1981. Change lines are shown as dashed lines. Lines D_2 and D_3 both represent the approximate front edge of the FTZ at these times, D_3 in fact being discontinuous in the horizontal.

The calculations of vertical velocity and vorticity are described in the Appendix and are representative of a horizontal scale of order 100 km. In these events there are one or two lines of cyclonic relative vorticity maximum ζ_{max} either near the forward part of the frontal zone and associated with the squall line, or towards the rear of the zone and corresponding approximately with the location of maximum boundary-layer baroclinity, the position analyzed on the synoptic scale as the surface cold front. Maximum values of ζ lie in the range f to $2f$, somewhat smaller than in the intense cold front studied in depth by Sanders (1955), where $\zeta_{max} \sim 9f$, but comparable with those in the recent case study by Ogura and Portis (1982), where $\zeta_{max} \sim f$. It is probable, for example, that larger vorticities (and indeed vertical velocities) exist on smaller horizontal scales. Values of $\zeta \sim 10^2 f$ in regions of the low-level jet were reported by Browning and Pardoe (1973; p. 635). In Event 2 the line of relative vorticity maximum associated with the cold air boundary slopes backwards with height, towards the cold air, as in the aforementioned case studies, but such a slope is not apparent in Event 4. In Event 3 a single line of maximum cyclonic relative vorticity with magnitude $\sim 1.5f$ corresponds with the squall line, whose passage is followed by strong ridging, but the cold air boundary remains at all times to the south of the array network. This would account for the region of anticyclonic vorticity following the squall line, with maximum value comparable with $-f$.

In Event 2, the time section covers a considerable period before the frontal passage. A prominent feature at these early times is the region of large anticyclonic vorticity, with $\zeta \sim -0.5f$ to $-f$, associated with a well-developed nocturnal jet.

The pattern of vertical motion shows broad similarity between events with ascent in at least the forward part of the frontal zone and subsidence behind. The structure in Event 4 approaches most closely that observed by Sanders (1955), Browning and Harrold (1970) and Ogura and Portis (1982), with a sharp jet of rising motion just ahead of the surface front. In the lowest 2 km, the maximum ascent rate is 0.2 m s^{-1}, although local values may considerably exceed this. In Event 3, strong ascent occurs just ahead of the pressure-jump line at about 1030 GMT.

In none of the events does there appear to be a marked relationship between the regions of maximum cyclonic vorticity and maximum horizontal convergence ($\partial w/\partial z$) as in earlier studies and this may be due to the essentially three-dimensional nature of the flow, especially in the frontal zone. It is not possible to select an orientation of the frontal zone such that along-frontal gradients are much smaller than cross-frontal gradients and where, for example, ζ is approximated by $\partial v/\partial x$ and the horizontal divergence by $\partial u/\partial x$. Accordingly, since quantities such as $\partial\zeta/\partial x$ and $\partial\zeta/\partial y$ are difficult to reliably estimate from the network array, we are unable to present a detailed vorticity budget diagnostic such as those given in the case study by Sanders (1955), or on the basis of model calculations by Blumen (1980).

b. *Frontogenesis fields*

A diagnostic which has been found useful in the study of fronts is the so called *frontogenesis function*, $D|\nabla_h\theta|/Dt$, first introduced by Petterssen (1936) and later extended to three dimensions by Miller (1948). It represents the material rate of change of the

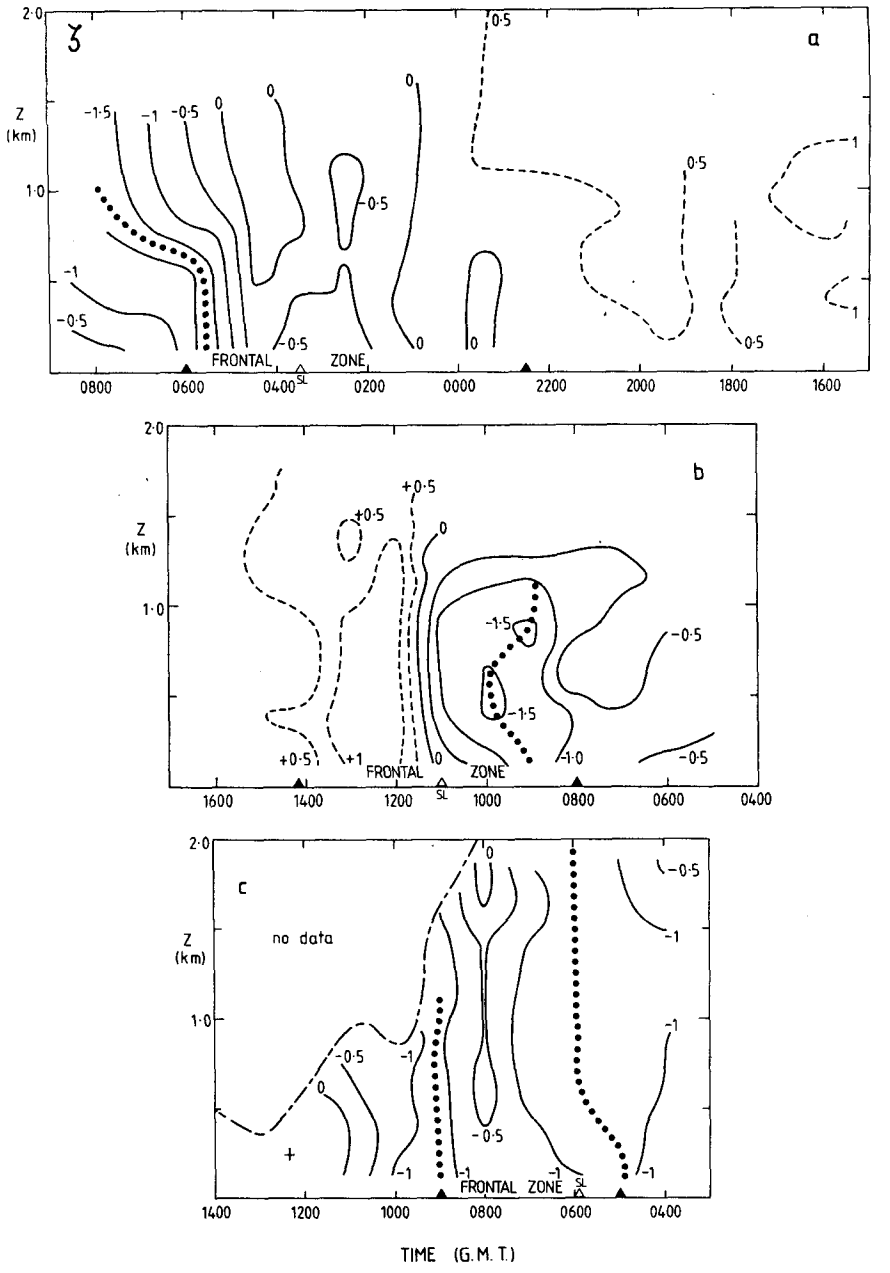

FIG. 9. Time-height cross sections of vertical vorticity $\xi(z, t)$ for three events: (a) Event 2, (b) Event 3 and (c) Event 4. Contours are labeled in units of 10^{-4} s^{-1} with negative values being cyclonic (appropriate to the Southern Hemisphere in conjunction with a right-handed system of coordinate axes with x pointing eastwards and y northwards), and dotted lines indicate local cyclonic vorticity maxima. Solid triangles at bottom denote position of initial and final "line"; open triangle, the position of main squall line (SL).

horizontal potential temperature gradient following air parcels along their three-dimensional trajectories. Starting from the entropy equation in the form $D\theta/Dt = \dot{q}$, it is algebraically straightforward to show that

$$\frac{D|\nabla_h\theta|}{Dt} = T_1 + T_2 + T_3 + T_4, \qquad (1)$$

where

$$T_1 = \hat{\mathbf{n}} \cdot \nabla_h \dot{q}, \qquad (2)$$

is the rate of frontogenesis due to gradients of the diabatic heating $\dot{q}$ in the direction of the horizontal temperature gradient $\hat{\mathbf{n}}$ $(=\nabla_h\theta/|\nabla_h\theta|)$,

$$T_2 = -\theta_z \hat{\mathbf{n}} \cdot \nabla_h w, \qquad (3)$$

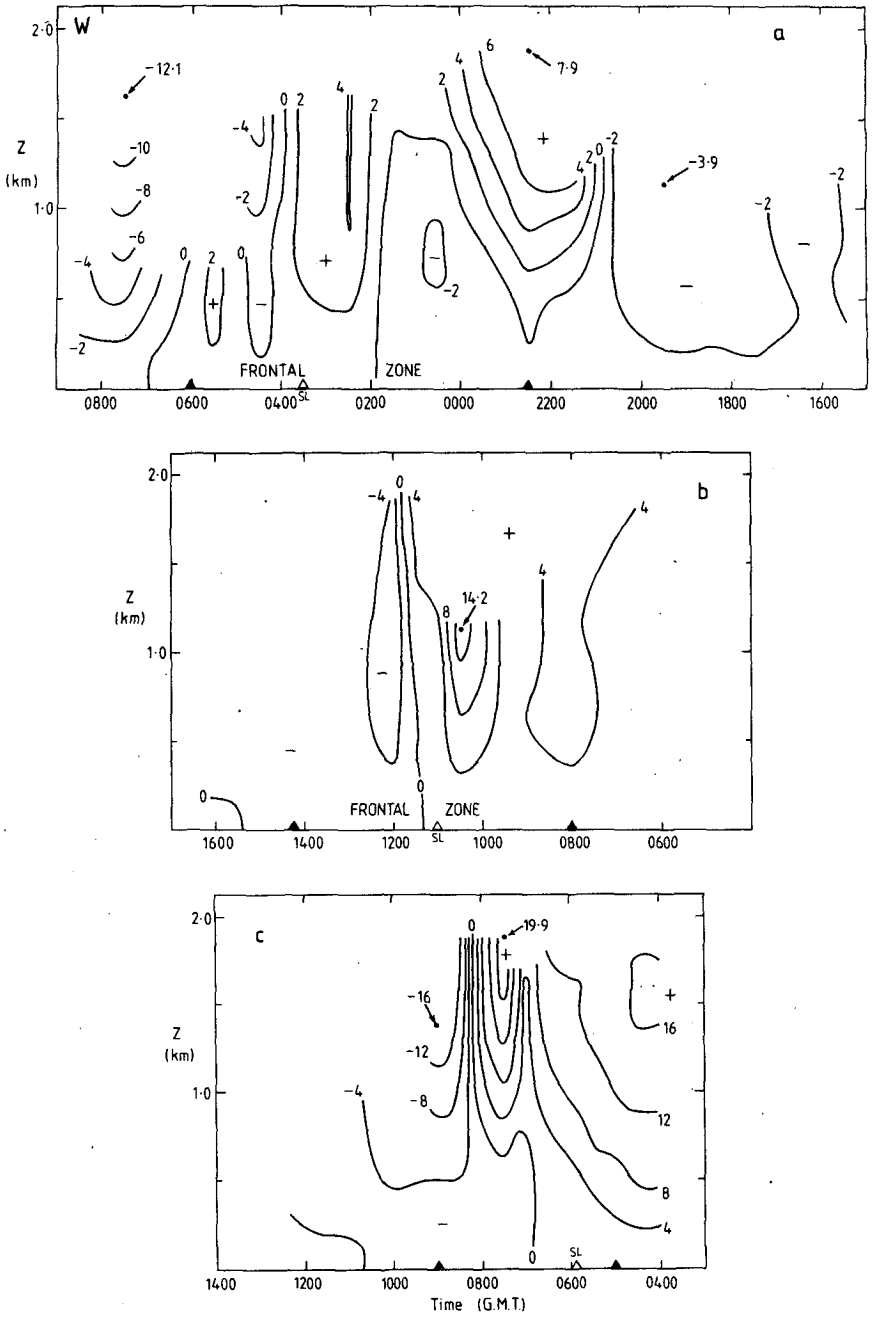

FIG. 10. As in Fig. 9 but for $w(z, t)$, with a contour spacing of 2×10^{-2} m s^{-1}.

is the rate due to the tilting of vertical gradients of potential temperature into the horizontal by the component of horizontal gradient of vertical velocity in the direction $\hat{\mathbf{n}}$,

$$T_3 = -\frac{1}{2} D|\nabla_h \theta| \tag{4}$$

is the rate of frontogenesis due to the horizontal convergence (measured by $-D$ where $D = u_x + v_y$) of potential isotherms, and

$$T_4 = \frac{1}{2} |\nabla_h \theta||\text{def}| \cos 2\beta, \tag{5}$$

is the rate due to horizontal deformation of the existing temperature field. In this expression, $|\text{def}| = (E^2 + F^2)^{1/2}$ is the total rate of deformation, $E = u_x - v_y$ and $F = v_x + u_y$ being the stretching and shearing deformation, respectively, and β is the angle in the horizontal plane between the dilatation axis and the potential isotherms. The analogous equation

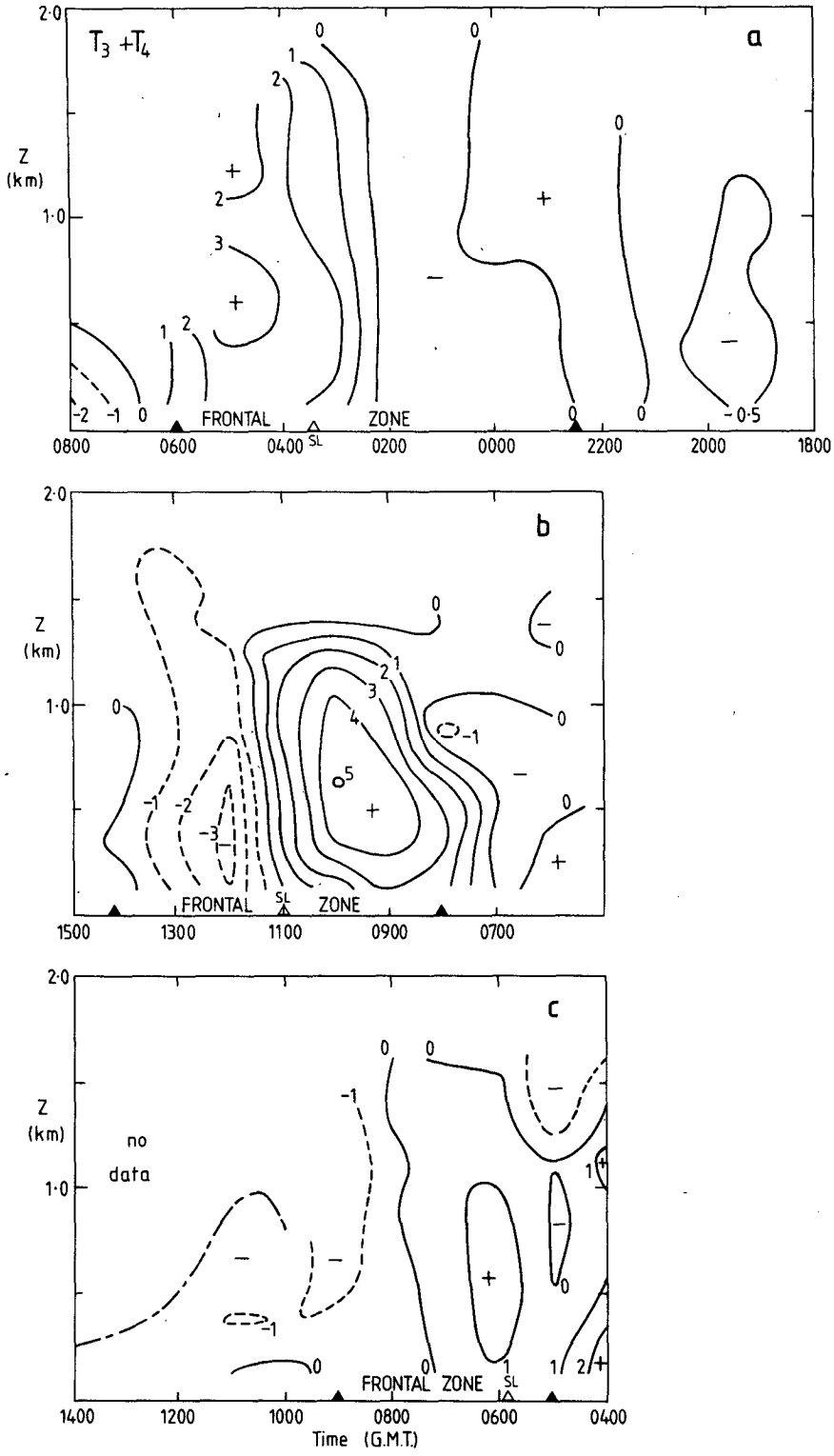

FIG. 11. Time-height cross sections of the rate of frontogenesis due to horizontal deformation and convergence, represented by the sum of terms T_3 and T_4 in Eq. (1), for three events. Contours are labeled in units of 10^{-9} K m^{-1} s^{-1}.

to (1) in pressure coordinates is used by Ogura and Portis (1982). In contrast, Sanders (1955) and Blumen (1980) use a slightly different form, appropriate when the along-frontal variation of all quantities, except possibly the large scale horizontal temperature gradient, can be ignored.

TABLE 2. Estimates of main terms in the frontogenetic equation 1 for 3 events, (Events 2, 3 and 4), for several time periods and averaging to a height of 1500 m.

Event	Time period (GMT)	Term (10^{-10} K m^{-1} s^{-1}) $\frac{\partial}{\partial t}\lvert\nabla_h\theta\rvert$	$U\frac{\partial}{\partial x}\lvert\nabla_h\theta\rvert$	$-w_x\theta_z$ sgn(θ_x)	T_3	T_4	Residual
2	2230–0200	2	0	−1	−1	1	3
	0200–0600*	20	−23	−1	8	2	−12
	0600–0900	1	11	−14	13	−12	25
3	0800–1100	13	−5	−5	10	6	−3
	1100–1500	−7	−10	−18	−4	−2	7
4	0500–0900	2	−23	−15	−3	8	11
	0900–1200	−4	−9	−8	−1	−3	−1
2 to 4	Transition zone	12	−17	−7	5	5	−8
	Post-frontal zone**	−4	−3	−13	3	−6	+9

* Active region of frontal transition zone.
** Includes post squall-line region for Event 3.

On the basis of data collected, it is not possible to calculate directly the diabatic term T_1 though it can be crudely estimated using a simple parameterization scheme discussed later. It is difficult also to estimate T_2 reliably since it involves the horizontal gradient of vertical velocity, itself a somewhat noisy field to estimate. It is possible, however, to determine time-height cross sections of T_3 and T_4 up to a height of 2 km.[4] These are believed to be the principal contributors to frontogenesis, at least on the synoptic scale (Hoskins and Bretherton 1972). Time-height cross sections of $T_3 + T_4$ are shown in Fig. 11 for Events 2, 3 and 4, respectively.

In all three events, $T_3 + T_4$ is relatively large and positive in the FTZ with maximum values confined to the lowest kilometer; this accords with the findings of Ogura and Portis (1982) and, essentially, of Sanders (1955). In Event 2, the magnitude of $T_3 + T_4$ is up to six times greater in the FTZ than in the prefrontal air. In all events, the horizontal deformation and convergence contributions are comparable in magnitude within the FTZ and elsewhere, but in the FTZ in particular they are not everywhere of the same sign. Generally, $T_3 + T_4$ is strongly frontolytic at low levels following the passage of either the squall line (Event 3) or D_f, the final line (Events 2 and 4).

Although the data are barely adequate for the purpose, we have made an attempt to estimate some of the other terms in Eq. (1). For each event the data are averaged over three layers (0–500, 500–1000 and 1000–1500 m) and for two or three time intervals, corresponding broadly with the pre- and post-frontal periods and the frontal transition zone period. In Event 3, two time periods were taken, one before and one after the passage of the squall line. For these time periods and layers we estimate, as well as T_3 and T_4, the contributions $\partial|\nabla_h\theta|/\partial t$ and $U\partial|\nabla_h\theta|/\partial x$ to the left-hand side of Eq. (1) ($\partial/\partial y$ could not be calculated through lack of data); the contribution $-w_x\theta_z$ sgn(θ_x) to T_2; and the residual required to make the estimate for $T_2 + T_3 + T_4$ on the right-hand side equal to the estimate for the left-hand side. As before, x is positive towards the east and thus approximately coincident with the direction normal to the front in Events 2, 3 and 4. Here we neglect all y variations.

The derivative $\partial|\nabla_h\theta|/\partial x$ is obtained by first computing $\nabla_h\theta$ for two arrays of stations using surface temperatures; array 1 is a "coastal" array and array 2 an "inland" array. Then the derivative is estimated manually from the two arrays, which have a mean separation of order 100 km. In all other terms, the "inland" array value alone is used for $|\nabla_h\theta|$. The mean advection velocity U is taken as the average for the five station wind finding array which overlaps both temperature arrays. In T_2, w is derived from the time-height cross sections at 3 or 4 hourly intervals for each 500 m thick layer. We assume then a time to space conversion with $\partial w/\partial x = -c^{-1}\partial w/\partial t$, where c is 15 m s^{-1}, an average speed for the various lines. Finally, the gradient $\partial\theta/\partial z$ is derived from the Mt. Gambier and Horsham radiosonde soundings and represents an average for the two stations for each 500 m thick layer and for each 3 or 4 hour period. As in earlier calculations, the overall values of terms (when time- and vertically averaged) incorporate a factor which reduces the surface $|\nabla_h\theta|$ used in the previous calculations (see Appendix). A summary of the term budgets for (1), averaged over the three 500 m thick layers, is presented in Table 2. The event average of terms for the frontal transition zone and post-frontal zone are included also in the table.

[4] For the purposes of calculation, the following equivalent expression for T_4 is preferred:

$$T_4 = -\tfrac{1}{2}(E\theta_x^2 + 2F\theta_x\theta_y - E\theta_y^2)/|\nabla_h\theta|.$$

The following broad conclusions can be drawn. The terms T_3 and T_4 are comparable in magnitude, though not necessarily of the same sign, and their sum is comparable with the local time derivative, $\partial|\nabla_h\theta|/\partial t$. The advective term $U\partial|\nabla_h\theta|/\partial x$ is predominantly negative, as one might expect in a coastal region with onshore flow, and so is T_2, and the magnitudes of both these terms are generally large compared with $T_3 + T_4$. The latter finding is consistent with one of Ogura and Portis (1982) who show that the tilting term field T_3 contributes significantly to the total rate of frontogenesis; moreover, this field is noisy compared with the fields T_3 and T_4 in contrast with model predictions (Blumen 1980).

Finally, the residual in Table 2 is consistent with estimates of the diabatic term T_1, interpreted as $\Delta H/(\rho C_p h \Delta x)$, where ΔH is the difference in surface heat flux H over distance Δx (~100 km) and h is boundary-layer depth (~1 km). Typically, with the final line at the center of the upper-air network at 1930 local time (Fig. 12), H will vary as follows: positive (~100 W m^{-2}) in the pre-FTZ region (clear skies); positive but near zero in the forward region of the FTZ (cloudy); positive (~100 W m^{-2}) to the rear of the FTZ (clear to partly cloudy skies) and near zero in the post-FTZ region under clear to partly cloudy skies over the sea. Thus we expect $\Delta H \approx -50$ W m^{-2} (100 km)$^{-1}$ within the FTZ ($T_1 \approx -5 \times 10^{-10}$ K m^{-1} s^{-1}) and $\approx +100$ W m^{-2} (100 km)$^{-1}$ post FTZ ($T_1 \approx +10 \times 10^{-10}$ K m^{-1} s^{-1}).

5. Low-level wind structure

Time-height cross sections of the wind field below 2 km reveal a number of significant features both within and outside the FTZ. A composite cross section based on 3 stations and 3 events is shown in Fig. 12, u' being normal to and v' parallel to the "front". The major features are identified as follows.

1) *Prefrontal nocturnal jet (A).* This feature at $x' = 300$ km is most probably the nocturnal jet, since it develops during the nighttime under generally clear skies in a stably stratified environment. For example, the observed time variations at $z = 525$ m are found to approximate calculations for a weakly-damped inertial oscillation when observed time variations in surface geostrophic wind are taken into account. The significance of this jet in relation to the dynamics of the FTZ itself is not yet clear.

2) *Prefrontal northerly jet (B).* Our case studies show maximum winds in the range 23–31 m s^{-1} at 1 km. These are related to increased horizontal pressure gradients in the vicinity of the initial line ($x' = 0$) which correspond with maximum surface geostrophic winds G_0 of about 25 m s^{-1}; i.e., winds at jet level are supergeostrophic by only several m s^{-1}. Horizontal traverses across the jet were made at 500 and 1500 m over the sea by the aircraft for Event 2 (Fig. 13). At 500 m the temperature rise to the west through the jet supports upper-air observations at a later time at Stations 3 and 5 which show a similar region of negative horizontal temperature gradient extending to approximately 2 km. The thermal wind opposes the surface geostrophic wind and, in concert with friction near the surface, favors a wind maximum at low levels.

Similar jets and associated regions of negative temperature gradient ahead of midlatitude fronts were found by Browning and Pardoe (1973) who

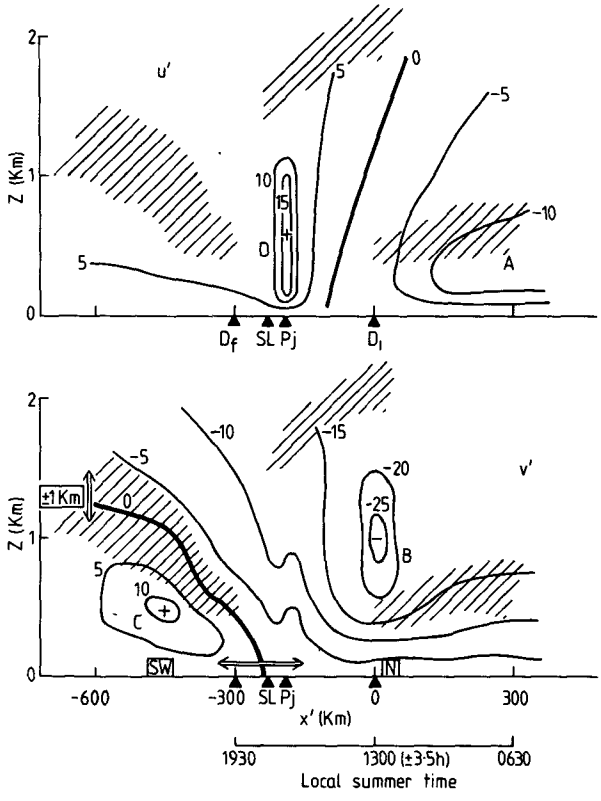

FIG. 12. Composite u' and v' cross section (z, t) from nine examples with isotachs at 5 m s^{-1} intervals; abscissa in local summertime and equivalent horizontal distance x' normal to the front [FTZ width = 6.5 (±2.5) h or 300 (±100) km assuming $x' = -ct$ and $c = 12.5$ m s^{-1}]. Time shown is relative to the time of arrival of the initial change line at the center of gravity of the 5 wind-station array (approximately 2 h later than at Station 6). Components u' and v' correspond approximately with components u (east–west) and v (north–south). See text for A to D. Maximum wind speeds with the observed range are as follows: (B) 27 ± 4 m s^{-1}; (C) 15 ± 3 m s^{-1}; (D) 15 ± 5 m s^{-1}; values of surface geostrophic wind beneath jets B and C are 22 ± 3 m s^{-1} (northerly) and 20 ± 4 m s^{-1} (southwesterly). Shaded areas correspond to strong vertical stability. For the v' field the vertical arrow indicates the likely variation (±1 km) in the vertical position of the $v' = 0$ isopleth at $x' = -600$ km. Thus for a vigorous cold air flow behind the FTZ, it may reach $z = 2$ km, while for a squall line with no cold air incursion, it may collapse to near the surface. Horizontal arrow in the region of squall line (SL) indicates the observed variation in the horizontal position of the $v' = 0$ isopleth, P_j denotes the position of the pressure jump.

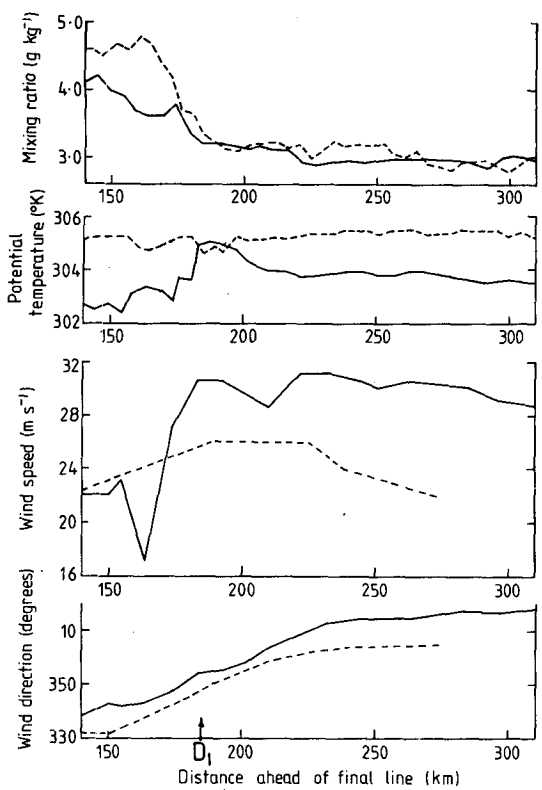

FIG. 13. Mixing ratio, potential temperature, wind speed and direction measured by the aircraft in the vicinity of the prefrontal jet (B in Fig. 12) of Event 2 over the sea west of Station 3 near the coast. Solid line denotes z = 500 m, dashed-line z = 1500 m. The abscissa is distance ahead of the final line D_f.

attributed such anomalous gradients to differential trajectories, i.e., the warmer air near the core of the jet originated from further south than that to the east of the jet. A similar mechanism is probable for fronts in southeast Australia, with the warmer air originating from further north over the continent than the cooler air to the east of the jet (Ryan and Wilson, 1985).

3) *Post-frontal southerly jet (C).* Maximum winds $\approx$ 12–18 m s^{-1} occur at $z \approx$ 0.5–1 km in the cold air behind the FTZ, a direct result of the intense positive horizontal temperature gradients in the presence of a southwesterly surface geostrophic wind. Thus it is a purely geostrophic phenomenon.

The physical basis for both prefrontal and post-frontal jets involves the opposition of surface geostrophic wind and thermal wind, and the influence of friction near the ground.

4) *FTZ westerly wind maximum (D).* This feature coincides with the propagating pressure-jump line; it is a dynamical response of the wind field to the narrow region of large pressure gradient, manifest as the pressure jump at any one location. Maximum values of horizontal pressure gradient [right-hand side of Eq. (6)] ranged over 10–30 m s^{-1} min^{-1}. With the pressure-jump line oriented approximately north-south, the result is a rapid rotation (backing) of the wind towards a westerly, representing flow out of the mesohigh, and a rapid increase in the u' component. The response extends to at least 1.5 km and produces, in addition, oscillations in v' at any one level. This overall behavior can be simulated by approximating the momentum equation to

$$\partial \mathbf{V}/\partial t \approx -\frac{1}{\rho}\nabla p, \tag{6}$$

where V is horizontal wind and ρ is air density. Equation (6) is solved to give $\mathbf{V}(t)$ for observed values of ∇p. A detailed examination of winds, particularly those near the surface, and their response to a sequence of pressure-jumps and pressure-falls, can be found in Garratt and Physick (1983).

For our observations we find in a broad region behind the pressure-jump line that

$$u \leqslant 0.75c_1,$$

where c_1 is the pressure-jump line velocity. This is consistent with observations of winds near the leading edge of gravity flows reported elsewhere. In fact, these, including some of our own near the surface, tend to show that $u - c_1 \geqslant 0$ only in a very narrow region where $|\nabla p|$ is a maximum, corresponding to a few minutes only at any one location (and therefore easily missed with ascents spaced 30-min apart).

6. Squall lines and pressure-jump lines

Goff (1976) and Wakimoto (1982) have discussed the evolutionary stages of thunderstorm outflows and the gust front from observations. These range from the early formative, through maturity, to the dissipating stage. Our examples of squall-line outflows correspond to the early mature stage (Event 2 and early stages of Event 3) through to the dissipating stage (late Event 3).

If the cold outflow penetrates to the surface, coincidence of the pressure jump and a temperature fall should occur. This is observed in practice, but when a surface-based inversion exists (as in Event 1 and Event 3) of sufficient "intensity," the cold-air outflow will not be sufficiently dense to reach the surface and will flow horizontally within an elevated layer.

Figure 14 shows vertical profiles of θ before and after the passage of a pressure-jump line on three squall-line occasions, illustrating the cooling associated with the outflow. The latter was typically 2–4 km deep (extends up to cloud base). Case A illustrates two additional features:

(i) lack of cooling below 250 m corresponds with the strong surface-based inversion;

(ii) partial warming on passage of the rear edge of the cold outflow corresponding with a pressure-fall line.

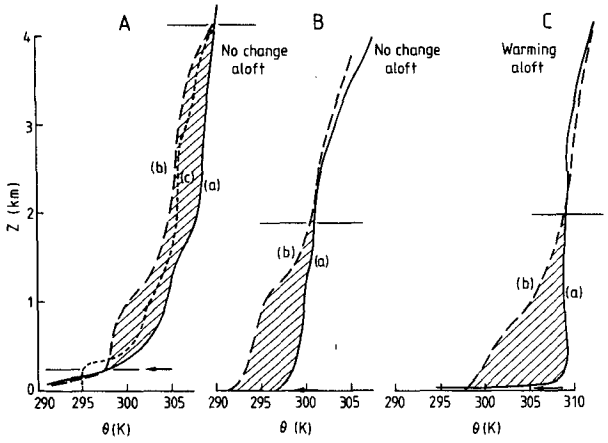

FIG. 14. Profiles of θ: (a) before and (b) after passage of the main pressure-jump line at either Station 3 or 5 for three events. Shaded regions represent the main region of cooling.

A: for Event 1 at Station 3 (a) at 1835 GMT (b) at 2035 GMT and (c) the sounding after the passage of the pressure-fall line, at 2235 GMT 26 November 1980. Pressure jump and pressure fall occurred at 1940 and 2100 GMT, respectively.

B: for Event 2 at Station 3 (a) at 0235 GMT and (b) at 0435 GMT on 23 November 1981. The pressure-jump occurred at 0315 GMT.

C: for Event 3 at Station 5 (a) at 1035 GMT level (b) at 1235 GMT 27 November 1981. Pressure-jump occurred at 1110 GMT. Horizontal arrows indicate lowest level of penetration of cooling.

We can calculate the induced surface pressure change Δp_0 corresponding to a temperature fall ΔT through a column of depth Δh and temperature $\bar{T}$. We have

$$\frac{\partial p_0}{\partial t} \approx -\left(\frac{gp_0}{R\bar{T}^2}\right)\Delta h \partial \bar{T}/\partial t, \tag{7a}$$

which, with $g/R = 0.034$ K m^{-1}, $\bar{T} = 288$ K and $p_0 = 1013$ mb, gives

$$\Delta p_0 = -0.415 \Delta h \Delta T, \tag{7b}$$

with Δp_0 in mb and Δh in kilometers. For the examples shown in Fig. 14 we find

Case	Calculated Δp_0 (mb)	Observed Δp_0 (mb)
A	4	2.5
B	2	1.5
C	4	2

where in case C significant warming in the layer 350–550 mb (of magnitude 2.2 K) reduces the calculated value of Δp_0 to 1 mb.

The main squall line has a motion V_s normal to its axis, determined in part by the midtropospheric wind $\bar{V}$. In contrast the pressure-jump line coincides with the downstream "nose" of a cold-air outflow which we assume moves as a density current. For a stationary squall line ($V_s = 0$) its features should resemble to a first approximation those of a simulated density current in 2D numerical models (e.g., Thorpe *et al.*, 1980), although there exist in the atmosphere complicating influences of vertical shear and low-level inversions, and those arising from the three-dimensional nature of the flow. The numerical simulations themselves have common features with laboratory flows (e.g., as described by Simpson and Britter, 1980). In a calm environment, the outflow velocity c should be given by

$$c = k\left(\frac{g}{\theta}\Delta\theta h\right)^{1/2}, \tag{8}$$

where k is a constant, $\Delta\theta$ the temperature deficit of the outflow relative to the environment and h the depth of the gravity flow following the "head". When $k = 1$, c is the so-called densimetric velocity c_*. The situation is represented schematically in Fig. 15a. In the presence of a tail or headwind, positive or negative V_0, respectively, laboratory, numerical and atmospheric examples (Simpson 1969; Simpson and Britter 1980; Thorpe *et al.* 1980) suggest that for zero environmental shear and a steady state two-dimensional system,

$$c = c_* + 0.7V_0, \tag{9}$$

where we assume $k = 1$. Variations of k reported in the literature, particularly those relating to atmospheric flows, are due to many factors including the use of Eq. (8) with the wrong value of h or with non-zero V_0, and the use of either Eq. (8) or Eq. (9) when the outflow source (thunderstorm or squall line) is moving (see Simpson 1969; Charba 1974; Wakimoto 1982). For a moving thunderstorm or squall line the relationship involving c and c_* would be expected to involve both V_0 and V_s. Here, for a three-dimensional system, we interpret the pressure-jump line as the locus of all individual Cb outflows (velocity c_0 in the direction of $\bar{V}$) with velocity c, more or less in the direction of V_s (see Fig. 15b).

For present purposes, we assume tentatively that the effect of V_s is in the same sense as V_0, so we take

$$c_1 = c_* + 0.7V_0 + \gamma V_s, \tag{10}$$

since γ need not necessarily equal 0.7, and where the outflow velocity is to be denoted by c_1. In practice, V_s will vary considerably (over a number of occasions) as will c_*, and hence c_1 and the relative positions of the pressure-jump line and squall line (see Fig. 16a, b). For any one event, the squall line itself may accelerate or decelerate, so that any one system is unlikely to be in steady state. An additional complicating factor lies in the identification of V_0 in a sheared flow, and a first approximation to this might be the u component averaged from the surface to a level $z = h$. Unfortunately we do not have V_0 available for all occasions. There does, however, seem to be a regular pattern to the low-level flow ahead of

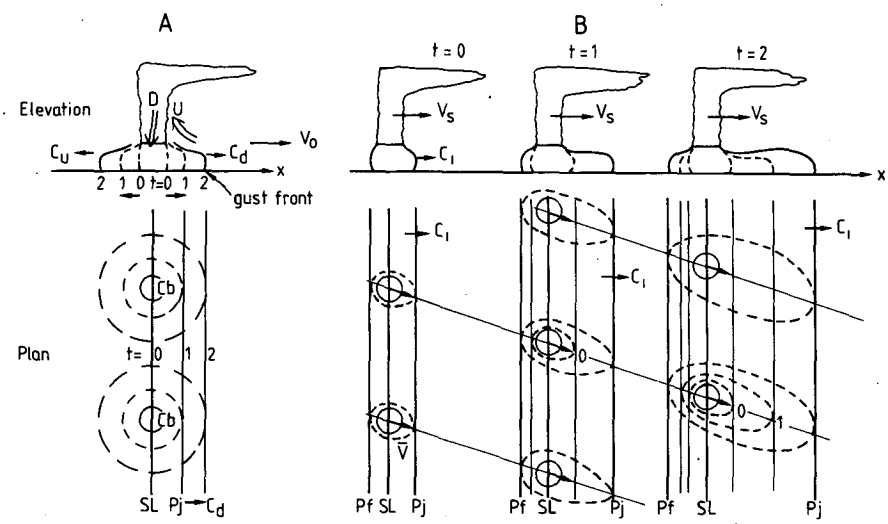

FIG. 15. (a) Schematic diagram of a stationary squall line showing a time sequence (t = 0, 1 and 2 units) of cold-outflow positions in a vertical section with the corresponding plan view of the Cb in the squall line (SL), together with the symmetrical outflow (for V_0 = 0) and the pressure-jump (p_j) line. Positions of the updraft (U) and the downdraft (D) are shown; V_0 is inflow velocity, C_d speed of the downstream front and C_u speed of the upstream front.

(b) As in (a) except for a squall line moving with a sufficiently large speed V_s so that the upstream gust front moves to the right and is seen as a pressure-fall (pf) line at any fixed location in space. The position (along x) is shown at three times, and due to translation of the squall line the outflow is shown as asymmetrical in plan view.

the squall line (see Fig. 12), and at this stage we let V_0 be constant in Eq. (10). We analyse this relation with c_* obtained by combining Eqs. (7a) and (8), with $k = 1$, to give

$$c_* = 10(\Delta p_0/\rho)^{1/2}, \tag{11}$$

with Δp_0 the pressure-jump amplitude in mb and ρ the air density in units of kg m^{-3}. Table 3 gives observed values of c_1, V_s, Δp_0 and c_*, and the relation between $c_1 - c_*$ and V_s is shown in Fig. 17. The excellent correlation supports the relevance of V_s and the role of the densimetric velocity, and hence the density-current nature of the cold air outflow producing the pressure jump. From the data analysis, we find in reference to Eq. (10) that $\gamma = 0.8$ and $V_0 \approx -8.5$ m s^{-1} with a variation in V_0 from occasion to occasion that is relatively small. This implied headwind is consistent with the composite cross section of the normal wind component shown in Fig. 12, if it is interpreted as the wind some 250 km ahead of the outflow prior to the region of main upflow. The near-equality of the coefficient $\gamma \approx 0.8$ with the laboratory-determined V_0 coefficient ($\approx$0.7) in Eq. (9) suggests that a suitable empirical relation for atmospheric flows, whether in steady state or not, is

$$c_1 = c_* + 0.7(V_0 + V_s), \tag{12}$$

i.e., the effect of the moving source is taken into account in a similar manner to a head or tail wind.

7. Discussion

a. Influence of the coastline

Berson *et al.* (1957, 1959) presented evidence for the influence of the coastal region on the speed of movement of the leading change line as a result of the daily cycle of differential heating between land and sea. Their observations of change lines were confined to the land, whereas we have additional evidence that the multiple change line nature of the FTZ exists also over the sea, consistent with the interpretation of these lines as convective instability lines. Table 4 summarizes, for the four main events, the origin and preferred region of development of the main change lines. In two of these the sea breeze *preceded* the arrival of the first convective line and in Event 4 may well have aided deep convection. In this case the sea-breeze penetration inland amounted to less than 50 km before it was overtaken by a convective line. Evidence for this line over the sea was provided by the aircraft in the form of a wind change and temperature fall at 500 m height beneath a band of altostratus at point A in Fig. 18a (at 0314 GMT). Farther south, the presence of Cb was indicated from radar. By 0420 GMT echoes were observed along the line over land (Fig. 18b), the rapid growth of the Cb in the coastal region suggesting the influence of sea-breeze convergence. A second convective line, identified by radar, and by the aircraft at B in Fig.

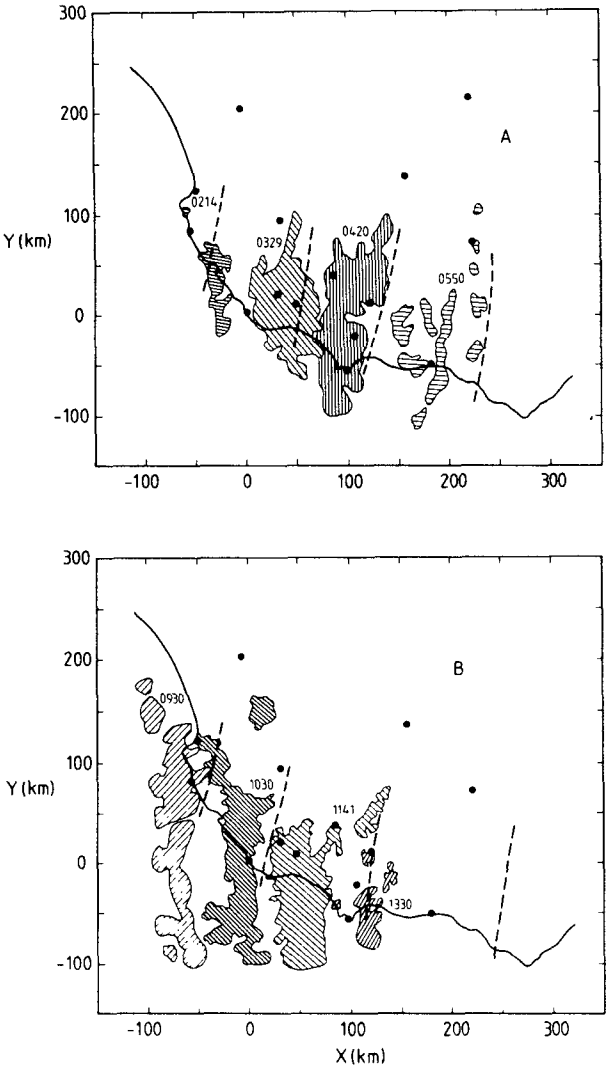

FIG. 16. Consecutive positions of the main radar echo region (main squall line) and the pressure-jump line (times are GMT.): (a) Event 2 (23 November 1981) and (b) Event 3 (27 November 1981).

18a, followed an hour later and developed into a major squall line near the coast.

The presence of a well-defined narrow zone of convergence some time before the onset of the first radar echoes has been reported by Ogura and Chen (1977). In this zone a strong horizontal gradient of temperature was provided by synoptic-scale confluence, and the subsequent vertical circulation generated by an inland sea-breeze-type mechanism (i.e., driven by a horizontal pressure gradient directed from moist to dry air across a dry line). In addition, the interaction between a sea-breeze circulation and cumulus-scale motion has been investigated numerically by Cotton *et al.* (1976) who found that significantly deeper and longer-lived precipitating clouds could be produced in a cumulus model when sea-breeze forcing was present. In regions favorable for deep convection on the basis of synoptic-scale criteria, development seems most likely to occur in subregions with identifiable mesoscale forcing; e.g., sea breezes, topographical features; or inland lakes (see e.g., Lewis *et al.*, 1974)).

Finally, differences in physical properties within the FTZ when this is situated over the sea and land can be expected. Thus for Event 2 (see Section 3.1) wind speed at 500 m is consistently lower over the land than over the sea, most likely the result of frictional effects. Additionally, lower temperatures over land are probably related to cooling through evaporation of rain, into air that would be initially drier over the land.

b. Conceptual model

The main results of analysis and interpretation of data, derived mostly from three events during Phase 2, with contributions from one event in Phase 1, are summarized schematically in Fig. 19. It should be emphasized that this conceptual model of the frontal transition zone (FTZ) in late spring and early summer is valid for a specific geographical region encompassing southeastern South Australia and western Victoria,

TABLE 3. Speed estimates and associated quantities relevant to four squall-line systems; data plotted in Fig. 17.

Event	Period (GMT)	c_l (m s^{-1})	Δp_0 (mb)	c_* (m s^{-1})	$c_l - c_*$ (m s^{-1})	V_s (m s^{-1})
1	1600–2100	12.0	2.5	13.6	−1.6	7
2	0329–0420	21.7	3.0	14.9	6.8	20
	0420–0550	19.4	1.5	10.4	9.0	20
3	0930–1030	21.7	3.0	14.9	6.8	15
	1030–1211	25.0	4.0	17.2	7.8	14
	1211–1330	16.9	3.0	14.9	2.0	9
	1330–1430	16.7	3.0	14.9	1.8	10
4	0424–0731	19.9	1.0	8.6	11.3	20
	0731–0924	24.3	1.0	8.6	15.7	25

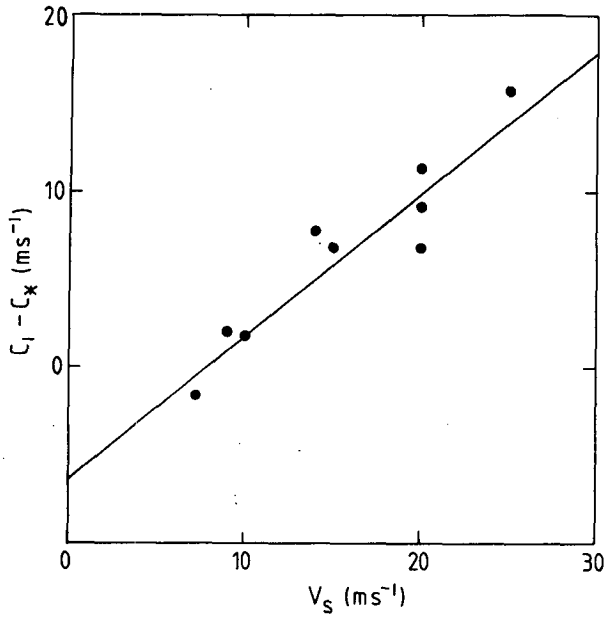

FIG. 17. Values of $c_1 - c_*$, c_1 the pressure-jump speed, plotted against the squall-line speed V_s. The least-squares regression is shown as a straight line through the data. Correlation coefficient r between $c_1 - c_*$ and V_s of 0.95 compares with $r = 0.75$ and 0.6 between c_1 and V_s, and c_* and V_s, respectively.

i.e., where many frontal systems first make substantial contact with the land. The more important features of the FTZ are given as follows:

1) The multiple line nature of the FTZ, reflecting to some extent the findings of Berson *et al.* (1957, 1959), is inferred from significant changes occurring in the wind, temperature, humidity and pressure at the surface over land. Analogous change lines are also evident from aircraft data over the sea and the land, at least to a height of 1500 m. Each change line, excluding the final line, is related to a line of organized convection, or convective instability line, identifiable as a mesoscale cloud band from satellite or as a rainband from radar.

2) Each line is associated with a pressure jump, excluding the final line and that associated with the onset of the sea breeze.

3) For seven examples there is a preferred time of arrival of the leading edge at the coastline, between 0400 and 1430 local time. During the latter half of this period sea breezes tend to occur as the leading change line.

4) The main component of the FTZ comprises one or two active squall lines, with associated pressure-jump and pressure-fall lines, and surface mesolow and mesohigh features. These mesofeatures produce a complex response in the low level winds with a large ageostrophic component.

5) The FTZ is characterized below 2 km by a prefrontal and weak post-frontal jet, both in approximate thermal wind balance along their axes. Within the FTZ, the wind field and circulation pattern are dominated by the main squall line, with *maximum* upwards vertical velocity $\approx$ 0.1 to 0.2 m s^{-1} ahead of the squall line and *maximum* downwards $\approx$ 0.1 m s^{-1} behind, both on a horizontal scale $\approx$ 100–200 km. Maximum cyclonic vorticity, in the layer $z \approx$ 500–1000 m, and boundary-layer baroclinity, are found to the rear of the FTZ.

6) Frontogenesis occurs largely within the FTZ in the Mt. Gambier region, with contributions from both low-level divergence and deformation.

The mesoscale conceptual model suggests that change lines move relative to each other, that interaction between lines may exist, and that variations in intensity and speed may occur in their travel eastwards. For example, there is evidence that (i) squall lines evolve in the coastal region, and (ii) the pressure-jump line will move far ahead of the squall line if the latter stalls. In the latter case the pressure jump, being associated with a wind shift and temperature fall, becomes ultimately the leading change line, and locally may take on the appearance of a dry "cool change" or "arrival of the front".

8. Conclusions

We have elaborated upon many of the features of summertime cold fronts described by Berson *et al.* (1957, 1959). One important difference concerns the interpretation of the leading change line. According to them, the origin of this line was nonfrontal and invariably accompanied by a pressure jump in the

TABLE 4. Geographic origin of main change lines for the four major events used in the study.

Event	Line	Origin over the sea	Developed just off the coast	Developed over land
1	D_1	✓		
	D_2	✓		
	D_f	✓		
2	D_1	✓		
	D_2	✓		
	D_3	✓		
	D_4	✓	✓	
	D_f	✓		
3	D_1			✓
	D_2			✓
	D_3			✓
	D_4	✓	✓	
	D_f	✓		
4	D_1			✓
	D_2	✓*		✓
	D_3	✓		
	D_f	✓		

* This line can be traced over the sea but its main development occurred over land.

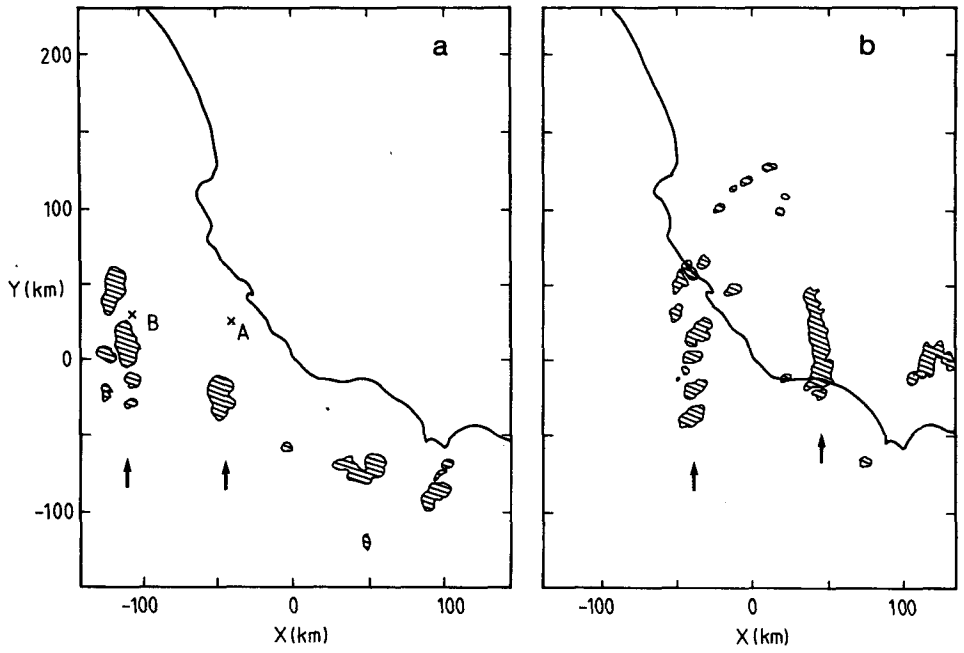

FIG. 18. Radar echoes defining two convective lines: (a) 0314 GMT and (b) 0420 GMT 2 December 1983. Points A and B in diagram (A) are referred to in the text.

absence of rainfall in the majority of cases. They concluded then that the jump and related wind shift were produced by a gravity wave traveling on the subsidence inversion, with the subsequent cooling being due to the advection of air of a continental origin which has had recent passage over the sea. The origin of the wave and pressure jump was seen more or less in the context of the theory of Tepper (1950). In contrast, our interpretation sees the leading change line, when there is no sea breeze present, as a convective instability line associated with a mesoscale cloud band, with cooling due to virga, or possibly as a vigorous squall-line outflow, with associated pressure jump, traveling well ahead of the squall line itself.

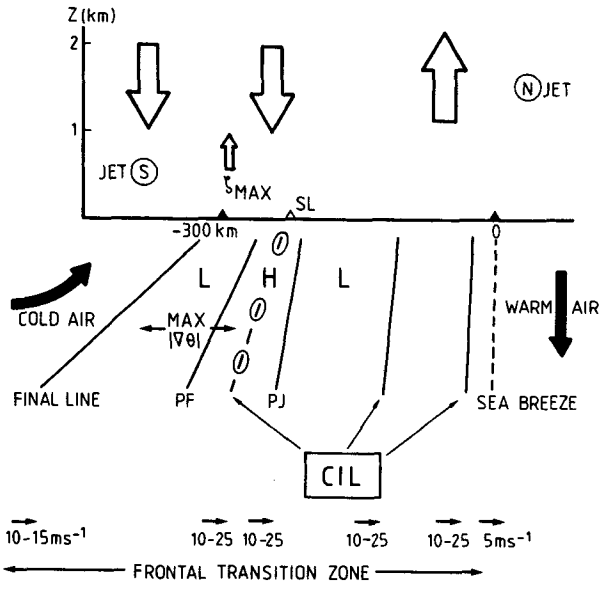

FIG. 19. Schematic diagram of the frontal transition zone. Main squall line, main pressure-jump line and main pressure-fall lines are denoted SL (dashed line, with open circles in horizontal plane), PJ and PF, respectively; the mesohigh and mesolow are denoted by H and L; CIL denotes convective instability lines, e.g., in the form of mesoscale cloud band, rainband and squall line, any of which may have an associated pressure jump. Open arrows in vertical plane represent direction of vertical motion, with their length approximately proportional to the magnitude of w.

In the context of overseas studies, we have found numerous features described elsewhere which may be integral components of the average summertime frontal system in southeast Australia. These include the prefrontal jet, squall lines and mesoscale rain bands. There is evidence of coastline influence upon the FTZ, and the basis for the development of squall lines from relatively weak convective lines is not yet explored.

One particular aspect of Australian fronts is worth emphasizing—that of the role of the hot, dry northerly flow, which is not usually found in the western United States or in the United Kingdom. This produces intense, low-level baroclinity in the frontal transition zone and, in the presence of the strong prefrontal jet, considerable advection of *dry* air into this zone. This has implications concerning the intensity of the cold outflow resulting from the evaporation of rain in the low-level air (with corresponding low rates of rainfall at the surface), and hence on the magnitude of the pressure jump and associated wind

shift. These aspects, together with the evolution of the FTZ in its passage eastwards along the coastal zone, are to be studied in a Phase 3 field experiment.

Acknowledgments. Many people who rendered assistance during Phases 1 and 2 by providing sites for instrumentation and making facilities available to the project team have been acknowledged in previous Technical Reports. Special mention should also be made of the technical and mechanical laboratory staff of the Bureau of Meteorology, CSIRO Division of Atmospheric Research, the University of Melbourne and both Monash and Flinders Universities.

Significant contributions to the data collection and analysis were made by Mr. D. Reid (winds), Mr. J. Stevenson (mesonetwork) and finally by Mr. P. Meighen (radar).

APPENDIX

Data Acquisition and Analysis

Table 1 summarizes the range of data which were available for the mesoscale study. Relevant aspects of the data acquisition and analysis are described.

1) *Surface data.* Surface variables (u, v, T, q, p) were determined as a time series at each station (where possible) with spacing of 30 min; this is consistent with the study of systems with a lifetime τ on the order of 3–9 h and velocity of translation $c \approx 15$ m s^{-1}, giving an equivalent space resolution $\sim$30 km in an array with average station spacing $\sim$75 km.

2) *Upper winds.* These were calculated as u (E–W component with W wind positive) and v (N–S component with S wind positive) at 50 m intervals (at heights 25 m, 75 m, etc.) vertically. Where necessary, components normal to and parallel to a change-line were readily determined (u' and v', respectively).

3) *Horizontal derivatives* (∇_h). Linear least-squares analyses applied to a minimum 4 or 5 station array gave $\nabla_h u$, $\nabla_h v$ and $\nabla_h T$ at the surface for several arrays, and $\nabla_h u$, $\nabla_h v$ at upper levels for the basic 5 station array shown in Fig. 1. In this case, where observations were not synchronous, linear time interpolation was used to give gradients each 30 minutes.

Analysis of the surface temperature field (θ_0) is important in that inferences on boundary-layer baroclinity in the frontal region can be made, and in addition, analysis of the frontogenetic process (Section 4) is made possible.

Representativeness of values of the surface temperature gradient $\nabla_h\theta_0$ for levels up to z = 1–1.5 km was assessed by comparing the temperature differences $\Delta\theta(z)$ as a function of height (z) between Stations 5 and 3 for several events. For Events 2, 3 and 4 we found that the correlation coefficients between $\Delta\theta(z)$ and $\Delta\theta(0)$ were typically between 0.5 and 0.9 for z up to 500–1000 m; in addition, $\Delta\theta/\Delta\theta(0)$ tended to decrease with height having mean values, 0.93, 0.83, 0.63 and 0.51 at z = 250, 500, 1000 and 1500 m, respectively. Where appropriate these values allow us to decrease calculated values of $\nabla_h\theta_0$ for estimates of $\nabla_h\theta(z)$, as for example, in the frontogenetic analysis in Section 4.

4) *Vorticity and vertical velocity fields.* The mean vertical velocity w for the five station array is obtained as a function of height by integrating the Boussinesq form of the continuity equation ($\nabla_h \cdot \mathbf{V}_h + \partial w/\partial z = 0$) with respect to z, and the vertical component of relative vorticity ζ is $v_x - u_y$. The fields of w and ζ so obtained are appropriate to the array scale, say Δx_A, which is of the order of 100 km. A smaller array size would be impractical, since the errors in horizontal wind determinations using rawinsondes or pibals must be considered to be at least ± 0.5 m s^{-1}, so that horizontal wind speed differences of at least a few m s^{-1} are required to estimate the horizontal divergence, and hence w, with an acceptable degree of accuracy.

5) *Mesoscale pressure field.* The mesonetwork contained 11 main stations giving p values each 30 min (every 3 min at 6 of these) appropriate to mesoscale analysis. Time-to-space conversion of "off-time" data along a chosen velocity vector $\mathbf{c}$ through each station generates 4–6 new data per station in the spatial domain (see station 8 in Fig. 1). The method, following Fujita (1963), assumes a steady state over the 2-3 h (maximum) that the conversion is performed and gives equal weight to each observation. In practice we use only ± 1 h "off-time" data when $c < 10$ m s^{-1}, because of the tendency for data to group around the station. In addition, where extrapolated data lie within 25 km of any other data, these are averaged. When $c > 20$ m s^{-1}, we use only data for $\pm$½ and ± 1 h, and for $10 < c < 20$ m s^{-1}, data out to ± 1½ h, at ½ h intervals are used. The method is probably less accurate than that devised by Barnes (1973), which weights observations according to their "age", interpolates to grid points and performs an objective contour analysis. In our case our generated data set does not have sufficient density in the northern part of the network for this objective scheme to be used, and the final p field is manually constructed with frequent reference to the detailed time series at 6 stations. In practice, fields were available for each event at 30 min intervals and were referred to mean sea level. These fields may use either absolute pressures (requiring correction for station bias, knowledge of station altitudes to ± 1 m and the use of actual screen temperature with an assumed lapse rate to determine column density) or a pressure perturbation such as described by Koch and McCarthy (1982) for meso-γ analysis. The latter involves linear regression analysis and it is impractical over time periods > 1–2 h, hence in meso-β analysis, particularly where pressure is varying in a highly nonlinear fashion with time. We use absolute pressure which allows the evaluation of geostrophic winds relevant in boundary-layer analysis.

REFERENCES

Barnes, S. L., 1973: Mesoscale objective analysis using weighted time-series observations. NOAA Tech. Memo. ERL NSSL-62, National Severe Storms Laboratory, 60 pp. [NTIS Comm-73-10781.]

Bennetts, D. A., and B. J. Haskins, 1979: Conditional symmetric instability—a possible explanation for frontal rainbands. *Quart. J. Roy Meteor. Soc.*, **105**, 945–962.

Berson, F. A., 1958. Some measurements on undercutting cold air. *Quart. J. Roy. Meteor. Soc.*, **84**, 1–16.

——, D. G. Reid and A. J. Troup, 1957: The summer cool change of south-eastern Australia. I. General Behaviour. Div. Meteor. Phys., Tech. Paper No. 8, CSIRO, Melbourne, 48 pp. [Available from The Chief, CSIRO Division of Atmospheric Research, Private Bag No. 1, Mordialloc, Victoria, 3195, Australia.]

——, —— and ——, 1959: The summer cool change of south-eastern Australia. II. Effects of differential heating and the modification of advective change. Div. Meteor. Phys. Tech. Paper No. 9, CSIRO, Melbourne, 69 pp. [Available from The Chief, CSIRO Division of Atmospheric Research, Private Bag No. 1, Mordialloc, Victoria, 3195, Australia.]

Blumen, W., 1980: A comparison between the Hoskins–Bretherton model of frontogenesis and the analysis of an intense surface frontal zone. *J. Atmos. Sci.*, **37**, 64–77.

Boucher, R. J., and R. Wexler, 1961: The motion and predictability of precipitation lines. *J. Meteor.*, **18**, 160–171.

Browning, K. A., and T. W. Harrold, 1970: Air motion and precipitation growth at a cold front. *Quart. J. Roy. Meteor. Soc.*, **96**, 369–389.

——, and C. W. Pardoe, 1973: Structure of low-level jet streams ahead of midlatitude cold fronts. *Quart. J. Roy. Meteor. Soc.*, **99**, 619–638.

Charba, J., 1974: Application of the gravity current model to analysis of squall-line gust fronts. *Mon. Wea. Rev.*, **102**, 140–156.

Clarke, R. H., 1961: Mesostructure of dry cold fronts over featureless terrain. *J. Meteor.*, **12**, 715–735.

Cotton, W. R., R. A. Pielke and P. T. Gannon, 1976: Numerical experiments on the influence of the mesoscale circulation on the cumulus scale. *J. Atmos. Sci.*, **33**, 252–261.

Elliott, R. D., and E. L. Hovind, 1964: On convection bands within Pacific coast storms and their relation to storm structure. *J. Appl. Meteor.*, **3**, 143–154.

Emanuel, K. A., 1979: Inertial instability and mesoscale convective systems. Part I: Linear theory of inertial instability in rotating viscous fluids. *J. Atmos. Sci.*, **36**, 2425–2445.

——, 1982: Inertial instability and mesoscale convective systems. Part II: Symmetric CISK in a baroclinic flow. *J. Atmos. Sci.*, **39**, 1080–1096.

Fritsch, J. M., and C. F. Chappell, 1980: Numerical prediction of convectively driven mesoscale pressure systems. Part II: Mesoscale model. *J. Atmos. Sci.*, **37**, 1734–1762.

Fujita, T. T., 1955: Results of detailed synoptic studies of squall lines. *Tellus*, **4**, 437–451.

——, 1963: *Analytical Mesometeorology: A Review. Meteor. Monogr.*, No. 27, Amer. Meteor. Soc., 77–125.

——, 1981: Tornadoes and downbursts in the context of generalised planetary scales. *J. Atmos. Sci.*, **38**, 151–153.

Garratt, J. R., and W. L. Physick, 1983: Low-level wind response to mesoscale pressure systems. *Bound. Layer Meteor.*, **27**, 69–87.

Goff, R. C., 1976: Vertical structure of thunderstorm outflows. *Mon. Wea. Rev.*, **104**, 1429–1440.

Held, G., 1977: Description of the unusual behaviour of a prefrontal squall line in South Africa. *J. Appl. Meteor.*, **16**, 651–653.

Hobbs, P. V., T. J. Matejka, P. H. Herzegh, J. D. Locatelli and R. A. Houze, Jr., 1980: The mesoscale and microscale structure and organization of cloud and precipitation in midlatitude cyclones. Part I. A case study of a cold front. *J. Atmos. Sci.*, **37**, 568–596.

Hoskins, B. J., and F. P. Bretherton, 1972: Atmospheric frontogenesis models: Mathematical formulation and solution. *J. Atmos. Sci.*, **29**, 11–37.

Houze, R. A., Jr., 1977: Structure and dynamics of a tropical squall-line system. *Mon. Wea. Rev.*, **105**, 1540–1567.

——, and P. V. Hobbs, 1982: Organisation and structure of precipitating cloud systems. *Advances in Geophysics*, Vol. 24, Academic Press, 225–315.

Hoxit, L. R., C. F. Chappell and J. M. Fritsch, 1976: Formation of mesolows or pressure troughs in advance of cumulonimbus clouds. *Mon. Wea. Rev.*, **104**, 1419–1428.

James, P. K., and K. A. Browning, 1979: Mesoscale structure of line convection at surface cold fronts. *Quart. J. Meteor. Soc.*, **105**, 371–382.

Koch, S. E., and J. McCarthy, 1982: The evolution of an Oklahoma dryline. Part II: Boundary-layer forcing of mesoconvective systems. *J. Atmos. Sci.*, **39**, 237–257.

Lewis, J. M., Y. Ogura and L. Gidel, 1974: Large-scale influences upon the generation of a mesoscale disturbance. *Mon. Wea. Rev.*, **102**, 545–560.

Lilly, D. K., 1979: The dynamical structure and evolution of thunderstorms and squall lines. *Annual Reviews of Earth and Planetary Science*, Vol. 7, Annual Reviews, 117–161.

Miller, J. E., 1948: On the concept of frontogenesis. *J. Meteor.*, **5**, 169–171.

Newton, C. W., 1950: Structure and mechanism of the prefrontal squall line. *J. Meteor.*, **7**, 210–222.

Ogura, Y., and Y.-L. Chen, 1977: A life history of an intense mesoscale convective storm in Oklahoma. *J. Atmos. Sci.*, **34**, 1458–1476.

——, and D. Portis, 1982: Structure of the cold front observed in SESAME-AVE III and its comparison with the Hoskins–Bretherton frontogenesis model. *J. Atmos. Sci.*, **39**, 2773–2792.

Orlanski, I., 1975: A rational subdivision of scales for atmospheric processes. *Bull. Amer. Meteor. Soc.*, **56**, 527–530.

Petterssen, S., 1936: A contribution to the theory of frontogenesis. *Geophys. Publ.*, **11**, 27 pp.

Ryan, B. F., 1982: A perspective of research into cold fronts and associated mesoscale phenomena in Australia into the 1980's. *Aust. Meteor. Mag.*, **30**, 123–131.

——, and K. J. Wilson, 1985: The Australian summertime cool change: Part III: Synoptic and mesoscale model. *Mon. Wea. Rev.*, **113**, 224–240.

Sanders, F., 1955: An investigation of the structure and dynamics of an intense surface frontal zone. *J. Meteor.*, **12**, 542–552.

Simpson, J. E., 1969: A comparison between laboratory and atmospheric density currents. *Quart. J. Roy. Meteor. Soc.*, **95**, 758–765.

——, and R. E. Britter, 1980: A laboratory model of an atmospheric mesofront. *Quart. J. Roy. Meteor. Soc.*, **106**, 485–500.

Smith, R. K., B. F. Ryan, A. J. Troup and K. J. Wilson, 1982: Cold fronts research: The Australian summertime "cool change". *Bull. Amer. Meteor. Soc.*, **63**, 1028–1034.

Tepper, M., 1950: A proposed mechanism of squall lines: The pressure jump line. *J. Appl. Meteor.*, **7**, 21–29.

Thorpe, A. J., M. J. Miller and M. W. Moncrieff, 1980: Dynamical models of two-dimensional downdraughts. *Quart. J. Roy. Meteor. Soc.*, **106**, 463–484.

Wakimoto, R. M., 1982: The life cycle of thunderstorm gust fronts as viewed with Doppler radar and rawinsonde data. *Mon. Wea. Rev.*, **110**, 1060–1082.

Wilson, K., and H. Stern, 1985. The Australian summertime cool change: Part I: Synoptic aspects. *Mon. Wea. Rev.*, **113**, 177–201.

Zipser, E. J., 1977. Mesoscale and convective scale downdrafts as distinct components of squall-line structure. *Mon. Wea. Rev.*, **105**, 1568–1589.